

# Analysis of very-high-resolution Galileo images and implications for resurfacing mechanisms on Europa

E.J. Leonard<sup>a,b,\*</sup>, R.T. Pappalardo<sup>b</sup>, A. Yin<sup>a</sup>

<sup>a</sup>Department of Earth, Planetary, and Space Sciences, University of California Los Angeles, Los Angeles, CA 90095-1567, USA

<sup>b</sup>Jet Propulsion Laboratory, California Institute of Technology, Pasadena, CA 91109, USA

## ARTICLE INFO

### Article history:

Received 18 October 2017

Revised 4 April 2018

Accepted 16 April 2018

Available online 17 April 2018

### Keywords:

Europa

Tectonics

Satellites/surfaces

Geological processes

## ABSTRACT

The young (<100 Ma) surface of Jupiter's icy satellite Europa raises the key questions: (1) what are the resurfacing mechanisms for creating Europa's young surface, and (2) how have these processes evolved through time? To address these questions we analyze the nine high-resolution frames obtained by the Galileo Solid State Imager (SSI)—eight at 16 m/pixel and one at 8 m/pixel (commonly quoted at the planned 6–12 m/pixel as in Greeley et al., 2000)—during the E12 flyby of Europa in Dec. 1997. This dataset is now two decades old, but it has not been analyzed in detail until this work. Despite the largely different viewing and lighting conditions, we mosaic these high-resolution frames into the 220 m/pixel regional context frame. We then perform geomorphologic mapping of the high-resolution image mosaic and the regional image frame, for comparison, and we also create a structural map of the high-resolution image mosaic. The units in the geomorphologic map are defined by surface texture, landform shape (morphology), dimension, and relative albedo. The structural map units include interpretations from the geomorphologic map units and their interpretation implies potential kinematic processes for the formation of particular structures. Our primary mapping observations include the regular spacing and gentle slopes of the ridge-and-trough terrain, the sharp boundaries and preserved structures of the chaos terrain, and the symmetry but irregular size of double ridges. We then evaluate proposed formation mechanisms for these and other mapped features. The high-resolution images also reveal an abundance of small (<100 m) pits, the presence of a newly identified high-albedo smooth material, and potential tectonic fabric, all of which have possible implications for the surface history. The mapping and structural analyses lead to the key finding that local-scale resurfacing mechanisms have transitioned from distributed deformation expressed by the formation of the ridged plains to discrete deformation characterized by the formation of chaos and isolated fractures. This finding is consistent with simultaneous ice-shell thickening and cooling occurring as the ice-shell deformed.

© 2018 Elsevier Inc. All rights reserved.

## 1. Introduction

Voyager and Galileo Solid State Imager (SSI) images of Europa reveal complex surface features exemplified by a wide variety of crosscutting surface structures with diverse morphologic expressions (e.g., Pappalardo et al., 1999). Additionally, the paucity of recognizable craters with diameters >10 km requires that Europa's surface is young, on the order of 60 Ma (Zahnle et al., 1998). Unraveling the cause of this young surface age combined with the complexity of Europa's surface features has led to competing hypotheses for the formation of key landforms—chaos struc-

tures, double ridges, and ridge-and-trough terrain. For chaos terrain these hypotheses include melt-through (Greenberg et al., 1999; O'Brien, 2002), diapirism (Pappalardo et al., 1998a; 1998b; Schenk and Pappalardo, 2004), and the collapse of a melt-lens within the ice shell (Schmidt et al., 2011; Soderlund et al., 2013); for double ridges, cryovolcanism (Fagents and Greeley, 1997; Kadel et al., 1998), tidal squeezing (Greenberg et al., 1998), linear diapirism (Head et al., 1999), shear heating (Nimmo and Gaidos, 2002), compression (Sullivan et al., 1998), wedging (Melosh and Turtle, 2004; Han and Melosh, 2010; Johnston and Montesi, 2014), and compaction (Aydin, 2006); and for ridge-and-trough terrain, extensional tilt-blocks (Kattenhorn, 2002), and folding (Leonard et al., 2015).

Although these competing hypotheses make specific predictions, their validation has been hampered by the lack of definitive observations due to the generally low-resolution images

\* Corresponding author at: Department of Earth, Planetary, and Space Sciences, University of California, Los Angeles, 595 Charles Young Drive East, Los Angeles, California, 90095-1567, USA

E-mail address: [erinleonard@ucla.edu](mailto:erinleonard@ucla.edu) (E.J. Leonard).

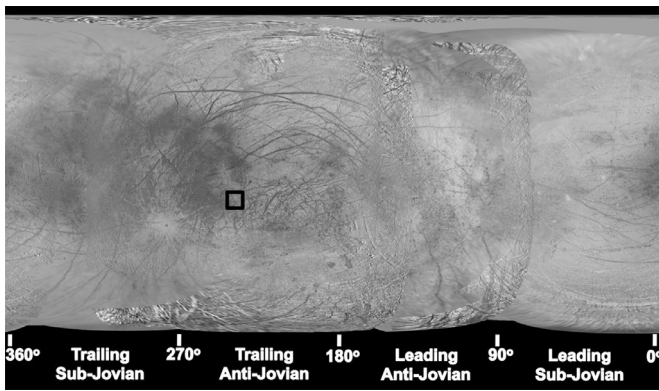


**Fig. 1.** The USGS Global mosaic of Europa in West positive coordinate system. The black box indicates the approximate location of the regional resolution image in Fig. 2(A). This area occurs between a chaos region (to the west) and a region characterized by bands and ridged plains (to the east, also known as the wedges region).

at  $>220$  m/pixel. In order to address this issue, we use the previously unanalyzed 12ESMOTTLE01 and 02 high-resolution (8–16 m/pixel, see Section 3.1) image strip to evaluate these hypotheses by refining the morphologic requirements or constraints on the surface feature formation mechanisms and thus narrow down the potential hypotheses. This work allows us to construct a geomorphologic map with the map units defined by surface texture, landform shape, dimension, and albedo. The geomorphologic map forms the basis for constructing a structural map, which correlates the mapped landforms to interpreted structures. This correlation in turn allows us to infer plausible kinematic processes for the observed morphologic features, leading to a better understanding of the resurfacing processes that have kept Europa's surface young.

The key findings of this work include: (1) Europa's surface deformation has transitioned from a distributed to a discrete mode over the discernable surface history, possibly resulting from the progressive cooling and thickening of the ice shell; (2) ridge-and-trough terrain exhibit gentle, quasi-symmetric slopes and regular spacing indicating folding as a likely formation process; (3) the consistent size and shape of double ridges along their length, but variation in size as a unit suggest compaction or linear diapirism formation mechanism, though neither appear to fit perfectly; (4) chaos terrain exhibits abrupt and heavily deformed boundaries with preserved pre-existing structures on the interior, favoring a water lens collapse formation mechanism; (5) secondary cratering processes may also contribute to resurfacing ( $\sim 0.5\%$  of the surface); (6) fine lineations are prevalent in the high-resolution images and are interpreted as a tectonic fabric; and (7) the presence of a newly identified *high albedo smooth* material may be indicative of a surface process operating at even a finer scale than is resolvable by the high-resolution images.

## 2. Regional geology

During its extended mission, the Galileo spacecraft imaged less than 0.03% of Europa's surface at 8–16 m/pixel, the highest resolution obtained of Europa's surface to date (Doggett et al., 2009; Greeley et al., 2000). One of the highest resolution imaged areas of Europa was obtained during Galileo's E12 flyby of the Trailing Anti-Jovian hemisphere (Fig. 1) and overlaps with an area imaged at regional resolution ( $\sim 230$  m/pixel during the E11 flyby (Fig. 2(A)). Previous work in the anti-Jovian hemisphere has been focused on the "wedges" region, Argadnel Regio (Schenk and McKinnon, 1989; Prockter et al., 1999, 2002), an area interpreted to have resulted from extensional tectonics (Helfenstein and Parmentier, 1983; Greenberg et al., 1998).

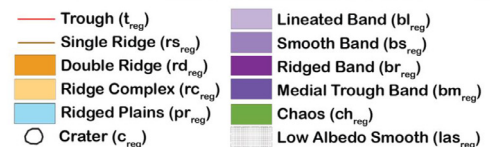
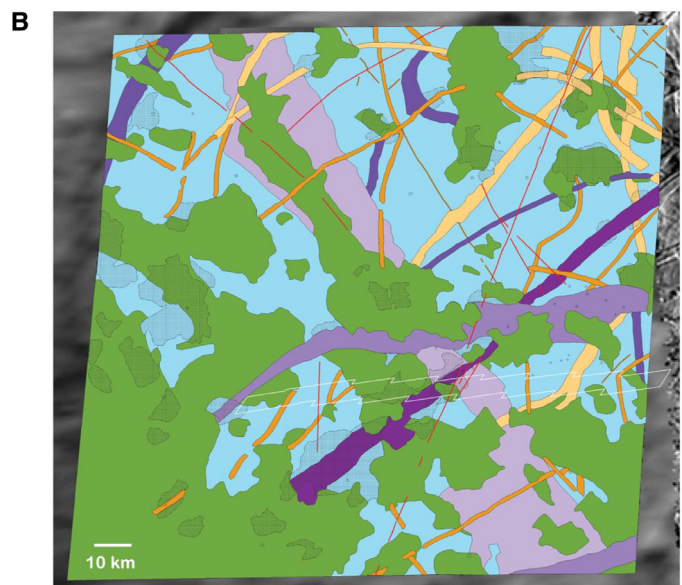
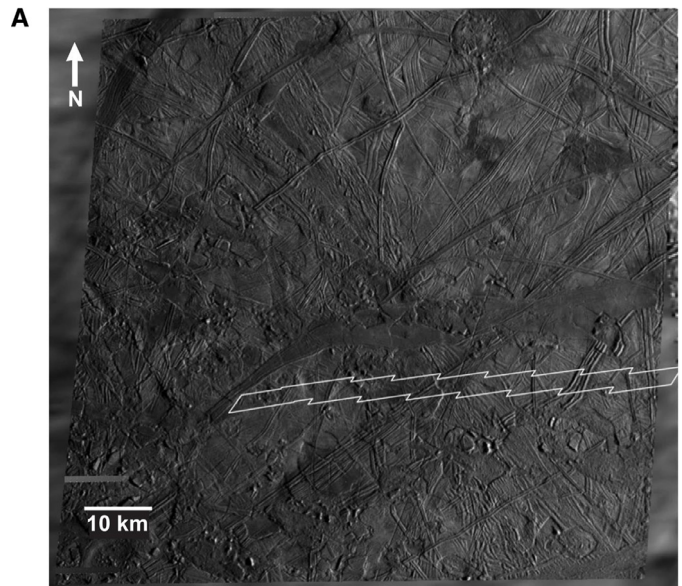


**Fig. 2.** (A) Regional resolution image (220 m/pixel) taken by Galileo SSI (11ES-REGMAP01 or 11E0017) with white outline indicating location of the high-resolution image mosaic (Fig. 3(A)). The image was taken at an incidence angle of  $74^\circ$  and an emission angle of  $23^\circ$ . Simple cylindrical projection, north is up. (B) Geomorphologic map of the regional resolution image (Fig. 2(A)) and corresponding key. The unit descriptions are in Section 4 and pictured in Fig. 4. The white outline indicates the location of the high-resolution image mosaic (Fig. 3(A)). Note the *lineated band* identified in the regional image that crosses through the high-resolution image mosaic (Section 7.2.6).

There are five primary terrain types identified on Europa (Figueredo and Greeley, 2000, 2004; Greeley et al., 2000): ridges, plains, chaos, bands, and crater terrain. This study region borders an area of chaos terrain to the west and an area of ridged plains terrain to the east, and therefore it is interesting to investigate as an area of terrain transition (Figs. 1, 2(A) and (B)); e.g., Figueredo and Greeley, 2004). Also, this transition in terrain type

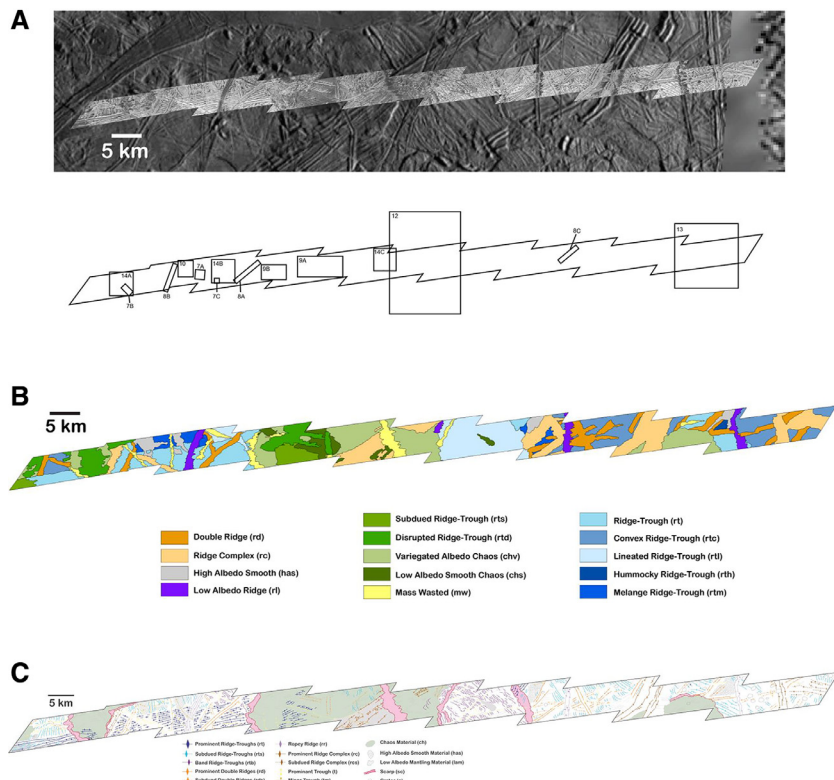


**Fig. 3.** (A) High-resolution image mosaic (top) made up of nine Galileo SSI frames (12ESMOTTLE01 and 02, images 2378r, 2400r, 2404r, 2407r, 2411r, 2418r, 2421r, and 2425r), the westernmost (2378r) at  $\sim 8$  m/pixel and the others at  $\sim 16$  m/pixel (see Table 1). The frames were imaged at an incidence angle of  $\sim 18^\circ$  and an emission angle of  $\sim 77^\circ$ . Simple cylindrical projection, north is up. Note that these images are not photometrically corrected. Outline of the mosaic (bottom) serves as a map of the locations of the other figures in this paper. (B) Geomorphologic map of the high-resolution mosaic (Fig. (A)) and corresponding key. The different material units identified are based on albedo, texture, apparent degradation, size and general morphology. The units are described in Section 4 and pictured in Fig. 4. (C) Structural map and key. For structural unit descriptions see Section 5. Multiple types of ridges and troughs are highlighted with different colors depending on the context in which they occur (e.g., within a band, as a set, or independently as a *double ridge*) as this has potential ramifications for formation mechanism and causes the ridges to vary in overall structure. Fault scarps are mostly contained to the border of chaos material regions, highlighting the sharp transition between chaos and surrounding terrain. Note the increasing amount of potential craters to the East. Symbols are based on Federal Geographic Data Committee Digital Cartographic Standard for Geologic Map Symbolization—Planetary Geology Features.

presents a wide variety of morphological terrain types in high-resolution (Fig. 3(A)) that could be applicable to many different areas on Europa, given that in general, chaos and ridged plains terrain cover the majority of the surface (Doggett et al., 2009; Greeley et al., 2000; Schenk, 2009). For instance, plains terrain, also identified as “ridged plains” as mapped by other investigators or “ridge-and-trough terrain” in this work, makes up  $\sim 60\%$  of Europa’s surface (Doggett et al., 2009).

### 3. Data and methods

In this work, we use nine frames of the highest resolution images in the E12 “Mottle” Region from the Galileo SSI Instrument, which have not previously been analyzed in depth. With this image mosaic we create geomorphological (Figs. 2(B) and 3(B)) and structural map (Fig. 3(C)) of the region in order to analyze the surface features and infer likely formation processes.

#### 3.1. Data

The high-resolution data in this region consists of nine frames—one at 8 m/pixel and eight at 16 m/pixel (a single Galileo SSI image at full resolution and eight subsequently acquired in summation mode)—all obtained at an incidence angle of  $16\text{--}19^\circ$  and an emission angle of  $74^\circ\text{--}76^\circ$  (Table 1; Fig. 3(A)). The resolution of these images is typically quoted to be 6 and 12 m/pixel respectively (e.g., Sullivan et al., 1999; Greeley et al., 2000; Prockter, 2004). In

fact, the planned, or estimated resolution was 12 m/pixel before the Galileo SSI captured the images. The actual resolution of the images, taken from the header of each image, noted in Table 1, is closer to  $\sim 8$  and 16 m/pixel, respectively, in the vertical direction and 40–50 m/pixel in the horizontal direction. The smear in the images is negligible at less than one pixel, based on the original E12 encounter planning data from JPL (D. A. Senske, personal communication). The regional resolution image that overlaps with the high-resolution images (Fig. 2(A)), from Galileo observation 11ES-REGMAP01, has a resolution of 229 m/pixel with an incidence angle of  $74^\circ$  and emission angle of  $22^\circ$ , essentially the opposite incidence and emission angles of the high-resolution observation (Table 1). A low incidence angle highlights albedo (reflectivity) differences, and a high incidence angle highlights structural features, and topography (Figs. 2(A) and 3(A)). Therefore, comparison between the high and regional resolution can be difficult, but provides complementary information. The images were corrected and mosaicked using the ISIS3 procedures *gllssi2isis*, *spiceinit*, *deltack*, *trim*, *cam2map*, and *mapmos*.

#### 3.2. Methods

We performed geological mapping of the high-resolution mosaic (Fig. 3(B)) prior to mapping the regional resolution image (Fig. 2(B)) in order to eliminate any biases that might come from prior analysis of the low-resolution images. Following analysis of the regional-context image, a consistency check was performed be-

**Table 1**  
Image data and information from all the images used in this study.

Orbit	S-clock	Observation ID	Incidence angle (°)	Emission angle (°)	Vertical resolution (m/pixel)	Horizontal resolution (m/pixel)
E11	s0420619278	11ESREGMAP01	74.617	22.338	229	228
E12	s0426272378	12ESMOTTLE01	19.917	76.307	8.0	23.4
E12	s0426272401	12ESMOTTLE02	19.130	76.505	16.8	49.2
E12	s0426272404	12ESMOTTLE02	18.836	76.444	16.6	49.6
E12	s0426272407	12ESMOTTLE02	18.502	76.125	16.6	48.0
E12	s0426272411	12ESMOTTLE02	18.164	75.915	16.4	47.6
E12	s0449962415	12ESMOTTLE02	17.834	75.544	16.3	46.4
E12	s0426272418	12ESMOTTLE02	17.5	75.275	16.3	45.6
E12	s0426272421	12ESMOTTLE02	17.171	74.843	16.0	44.3
E12	s0426272425	12ESMOTTLE02	16.850	74.529	15.5	43.5

\*Note the phase angle is relatively constant between the images ( $\sim 60^\circ$ ).

tween the two maps, regional and high-resolution. The differences noted—viewing geometry effects, misidentified chaos, and insights to band formation—are analyzed in Section 7.2. This method of mapping the high-resolution images first, without any context, is not commonly practiced in planetary mapping given that images of the same surface typically improve in resolution over time so low-resolution maps are typically followed sequentially by high-resolution maps (e.g., Lucchitta and Soderblom, 1982; Doggett et al., 2009). By reducing any low-resolution mapping bias, we offer a unique perspective on the classification of geomorphologic features observed at high-resolution based on their texture and morphology, which can have implications for their formation mechanism.

Based on the geomorphologic map, we also constructed an interpreted structural map of the same high-resolution region (Fig. 3(C)). The structural map is different from the geomorphologic map in that it relates the observed landforms to specific structures, and implies a kinematic process of ice-shell deformation that can lead to the formation of the observed surface features. A key assumption in constructing the structural map is that the surface erosion is negligible, and the landforms preserve the original shape of the structures resulting from ice-shell deformation. Post-emplacment relaxation, deformation, sublimation, and down slope failure, could affect the original structure post-formation, so the assumption has limits (Moore et al., 1999; Moore et al., 2009; Section 7.1.5). Though it is typical to combine the geomorphologic and structural maps together, we do not do this for this region due to its tectonic complexity of the terrain and to include details without making the maps too busy or cluttered. Unlike the geomorphologic map, the interpreted structural map integrates inferences from regional resolution map (e.g. *band ridge-and-troughs*, Section 5.1.7).

In order to place detailed geomorphologic and structural maps in a regional context, we also create a regional-scale geologic map (Fig. 2(B)). Comparison between the maps at different resolutions over the same area provides insights into the nature of the first-order features common on Europa. The regional map combines the geomorphologic and structural mapping techniques employed in the high-resolution maps. The image frame (9278r) from which we derive the regional map was previously mapped, but in less detail (Figueredo and Greeley, 2004) than in this study.

#### 4. Geomorphologic map and units

The main focus of this work is to map European surface features at the highest resolution available in this morphologically transitional region—from chaos dominated to ridge dominated terrain—in order to analyze potential surface feature formation mechanisms and create an inferred evolutionary sequence. Creating a geomorphologic map (Fig. 3(B)) provides insight into the potential similarities and differences of surface features across the narrow high-

resolution strip, and this permits direct comparison to the regional resolution data in the area.

The definition of major geomorphologic mapping units adopted for the high-resolution observations is based on the previous work done in this region using the regional resolution images (Figueredo and Greeley, 2004) but modified for the high-resolution as appropriate. The mapping units for the relevant regional resolution image and map (Fig. 2(B)) are denoted with a “reg” subscript (ex.  $t_{reg}$  for troughs in the regional resolution). Units containing a “low albedo” description could be analogous of “dark” terrains with albedos measured between 0.17–0.6, as compared to the “bright” terrains with albedos typically  $>0.7$  (e.g., Helfenstein et al., 1998). Examples of all of the geomorphologic units adopted can be found in Fig. 4.

##### 4.1. Ridge units

Though there is much variation in specific expression, ridge material generally consists of a topographically high quasi-linear landform. There may also be an associated trough or troughs running sub-parallel to the ridge or ridges. Different sub-units of ridge materials can grade into one another along a ridge’s length, making it difficult to classify and further complicating the inferred origin of these landforms.

##### 4.1.1. Double ridge unit ( $rd, rd_{reg}$ )

Double ridges consist of two subparallel quasi-linear topographically high landforms of relatively high-albedo. The landforms are rounded to triangular in cross-section and separated by a trough that commonly contains low albedo material. The width of each ridge pair can vary from  $\sim 400$  to  $\sim 1200$  m, making double ridge width relatively consistent on the regional scale, but variable on a local scale. This identified morphology is the same in the high-resolution ( $rd$ , Fig. 4(d)) and regional-resolution maps ( $rd_{reg}$ , Fig. 4(c)). An important additional note is that structures that appear to be *double ridges* in the regional resolution ( $rd_{reg}$ ) are actually identified differently, e.g. revealed as *ridge complexes* (see Section 4.1.2), in the high-resolution images.

##### 4.1.2. Ridge complex unit ( $rc, rc_{reg}$ )

Ridge complexes are intricate and varied landforms that consist of a series of irregularly spaced ridges and troughs (Fig. 4(f)). The ridges may vary from linear to curvilinear and bifurcate along their lengths in some cases. As a sub-unit, *ridge complexes* still carry great diversity in size (from  $\sim 500$  m to  $>10$  km in width) and shape (ridge flanks range from steep and straight to gently convex). In the regional resolution data ( $rc_{reg}$ , Fig. 4(e)), part of the *ridge complex* can split or join along its length (e.g., Head et al., 1999; Figueredo and Greeley, 2000).

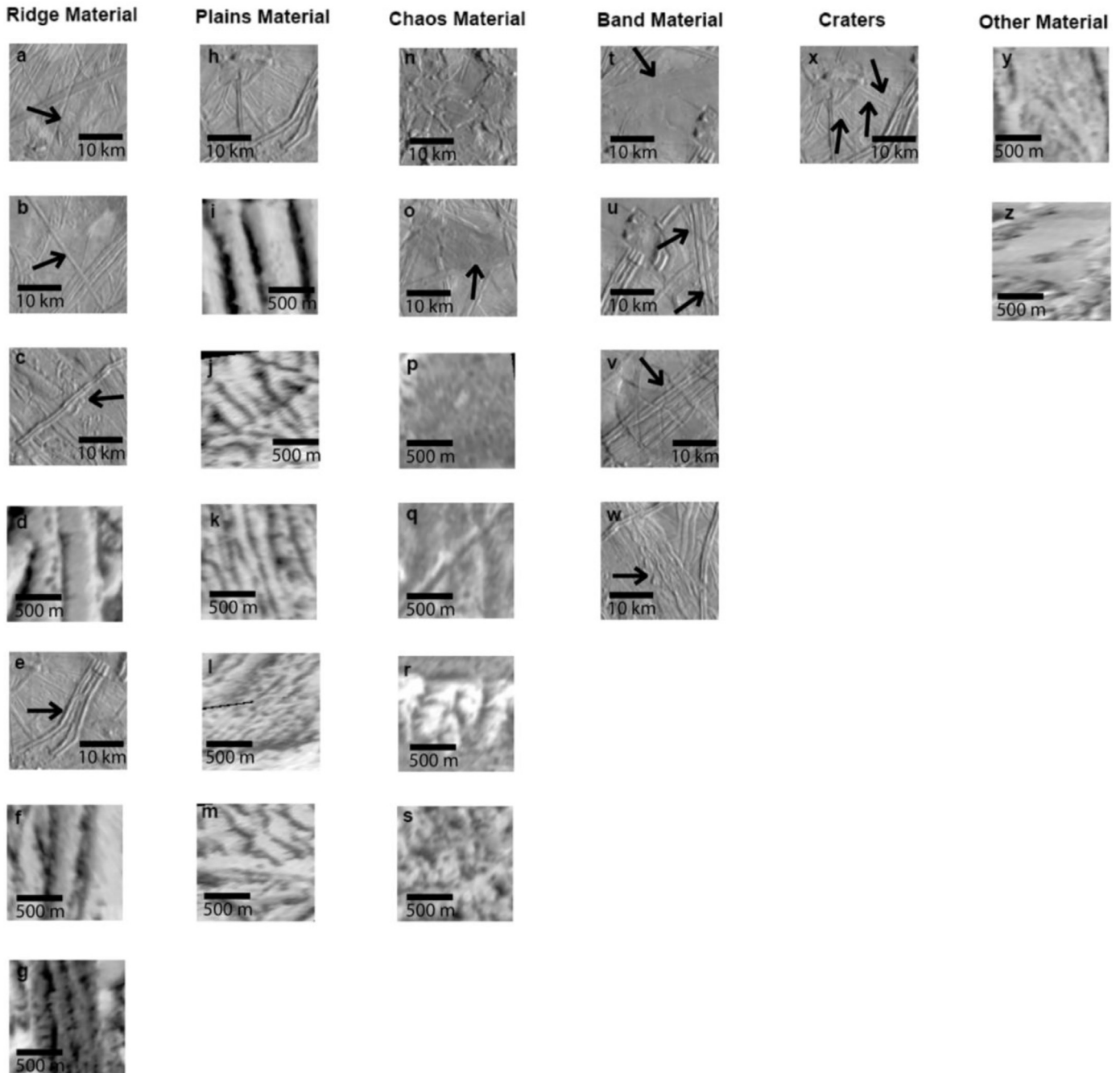


**Fig. 4.** Classification of material units based on geomorphology, texture, albedo and size. For unit descriptions and interpretations see Sections 4–7. Both regional resolution and high-resolution units for the geomorphologic maps are included (see corresponding scale bars). For the Ridge Material or material associated with ridges that were not a part of a set or system, there are *troughs* (a), *double ridges* at regional resolution (b) and high resolution (c), *ridge complexes* at regional resolution (d) and high resolution (e), and *low albedo ridges* (f). For the Plains Material, or ridge-and-troughs material, there are *ridged plains* (h), *subparallel* (i), *convex* (j), *lineated* (k), *hummocky* (l), and *mélange* (m). For the Chaos Material, there is a general *chaos* unit for regional resolution (n) as well as a *low albedo mantling* (o), and for high resolution, *low albedo smooth* (p), *subdued ridges* (q), *discontinuous* (r), and *variegated* (s). Band Material is identified only in the regional resolution and includes *smooth* (t), *medial trough* (u), *ridged* (v) and *lineated* (w). There are a few *craters* in the regional resolution (x) and other units, which do not fall under the main five categories including *high albedo smooth* (y) and *mass wasted material* (z).

#### 4.1.3. Low albedo ridge unit (rl)

The low albedo ridge unit is similar to double ridges (Section 4.1.1) and ridge complexes (Section 4.1.2) but consists mostly or completely of a low albedo material. In contrast to double ridges and ridge complexes where low albedo material is confined to the troughs, a low albedo ridge is either made of or coated in a similar low-albedo material. Though similar in morphology, the low albedo ridges are smaller in size than ridge com-

plexes; its ridge surfaces are also characterized by a ropy texture or more rounded ridge tops. These ridges have been identified only in the high-resolution region (Fig. 4(g)), though this could be due to the incidence angle differences between the regional and high-resolution images: The low incidence angle of the high-resolution images highlights albedo differences, causing the low albedo ridges to appear prominent or could be due to limb darkening, whereas the high incidence angle of the regional resolution image high-

lights topography and conceals the albedo differences between different landforms. The phase angle between the regional and high-resolution images, which could also influence albedo variations, remains relatively constant ( $59^{\circ}$ – $61^{\circ}$ ) so this is likely not the source of the appearance of the *low albedo ridges*.

#### 4.1.4. Trough unit ( $t_{reg}$ )

Troughs are topographically low quasi-linear landforms that have a low albedo appearance in the images. These depressions appear to have steep sides and v-shaped cross sections, though they are on the border of what is resolvable in the regional resolution. They are identified in the geomorphological map at regional resolution (Fig. 4(a)) and in the structural map at high resolution (Section 5.2.2).

#### 4.1.5. Single ridge unit ( $rs_{reg}$ )

Single ridges consist of one high-albedo topographically high landform with a lack of central topographic low or trough (Fig. 4(b)). These features tend to be linear and rounded in cross-section. *Single ridges* can transition into other types of ridge terrain along their length including *double ridges* (Section 4.1.1) or *ridge complexes* (Section 4.1.2).

### 4.2. Plains units

The plains units are characterized by a series of small-scale ( $\sim 200$ – $500$  m in width) high-albedo ridges which can be anywhere from sub-parallel to overlapping, and in several cases in multiple orientations. The individual ridges do not exceed  $\sim 100$  m in topographic relief, and average closer to 60 m from trough to ridge crest (Leonard et al., 2015). The most striking characteristic of plains material (also known as ridged plains, background plains, and ridge-and-trough terrain) is that it is one of the oldest units on Europa's surface because it falls in the stratigraphic background relative to essentially every other feature (Greenberg et al., 1998; Doggett et al., 2009; Pappalardo et al., 1999; Prockter et al., 1999; Greeley et al., 2000; Figueredo and Greeley, 2004). Plains material covers  $\sim 60\%$  of Europa's surface (Doggett et al., 2009; Greeley et al., 2000), but has not been examined in detail as the ridges within it are at a sufficiently small scale and very high-resolution data ( $< 40$  m/pixel) covers  $< 0.03\%$  of the surface.

#### 4.2.1. Subparallel ridge-and-trough unit ( $rt$ )

The ridge-and-trough unit consists of systematic, quasi-linear sets of ridges, topographically high landforms, alternating with troughs, or topographically low regions (Fig. 4(i)). The ridges are rounded to triangular in cross-section, and have a topographic wavelength of  $\sim 300$ – $500$  m. The limited extent of the high-resolution data does not allow us to observe the exact number of ridges within this unit. The ridges are also observed to be curvilinear and pinch and swell in width along trend (for example, Fig. 5, left panel). In various areas, the ridges or associated troughs bifurcate along their lengths and in this way add another ridge or trough to the system.

#### 4.2.2. Convex ridge-and-trough unit ( $rtc$ )

The convex plains unit has smaller ridge spacing than *subparallel ridge-and-trough* unit (see Section 4.2.1),  $\sim 300$ – $350$  m, and these ridges are exclusively rounded in cross-section (Fig. 4(j)). Ridges can pinch and swell and bifurcate in some cases. This unit has been previously identified by Patel et al., (1999a) in the Galileo 12ESWEDGES 01/02 observation within Argadnel Regio (Fig. 5).

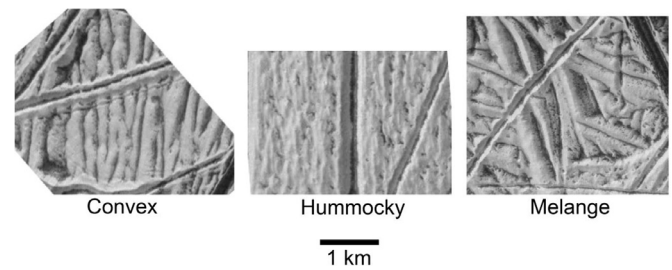


Fig. 5. These three ridged plains sub-units—*convex*, *hummocky*, and *mélange*—were first identified by Patel et al., (1999a). These results were never published in a peer-reviewed journal, but we choose to recognize this work here, as it is the only other work to analyze the varying morphologies within the broad European ridged plains unit using high-resolution ( $< 50$  m/pixel) images provided by the Galileo mission. For these units, we adopt or slightly modify Patel's et al. material and structural description. The other ridge-and-trough units described in this work are heavily modified or unique compared to those in Patel et al.

#### 4.2.3. Lineated ridge-and-trough unit ( $rtl$ )

This lineated unit contains ridges and troughs that are roughly subparallel to one another with a topographic wavelength varying from  $\sim 100$ – $300$  m (Fig. 4(k)). The ridges are sharply chevron shaped in cross-section and have steep sides compared to the other ridged plains units.

#### 4.2.4. Hummocky ridge-and-trough unit ( $rth$ )

The hummocky plains unit (Fig. 4(l)) is characterized by small-scale ridges and troughs which commonly pinch and swell along their length (Fig. 5; Patel et al., 1999a). They are on the verge of what is clearly identifiable in this high-resolution image mosaic, but they have a topographic wavelength of  $\sim 50$ – $100$  m.

#### 4.2.5. Mélange ridge-and-trough unit ( $rtm$ )

The *mélange* ridge-and-trough unit (Fig. 4(m)) consists of cross-cutting ridges and troughs in various directions (Fig. 5; Patel et al., 1999a). The ridges typically are rounded in cross-section and do not exceed  $\sim 300$  m in topographic wavelength and are typically closer to  $\sim 150$  m in topographic wavelength.

#### 4.2.6. Ridged plains, undivided ( $pr_{reg}$ )

The undivided ridged plains are only termed and mapped as such at the regional resolution, where it is usually used as a general term for any bright region containing small crosscutting lineaments, which are barely resolvable (Fig. 4(h)). Undivided *ridged plains* could consist of various crosscutting double ridges or systematic subparallel to curvilinear sets of ridges and troughs.

### 4.3. Chaos units

Chaos, in general, is characterized by blocks of crustal material, ranging from tens of kilometers to tens of meters in size, within a low albedo hummocky matrix (Doggett et al., 2009; Greeley et al., 2000; Kattenhorn and Hurford, 2009). It is a disrupted terrain inferred to be associated with higher heat flow with respect to the surrounding terrain or perhaps in contact with the subsurface ocean (e.g., Greenberg et al., 1999; Pappalardo et al., 1999; Greeley et al., 2000). Lower albedo material on Europa typically has a higher concentration of non-ice material and is commonly inferred to have originated in the subsurface ocean (Shirley et al., 2010; Dalton et al., 2012).

#### 4.3.1. Low albedo smooth chaos unit ( $chs$ , $las_{reg}$ )

The low albedo smooth unit is identified in the high resolution ( $chs$ , Fig. 4(p)) as a unit with lower albedo than the surrounding features and with unresolvable roughness within the chaos terrain.

The material appears smooth down to the scale of a few high-resolution pixels ( $\sim 20\text{--}40$  m).

Occurring primarily near the chaos regions in the regional resolution, *low albedo smooth* ( $las_{reg}$ , Fig. 4(o)) refers to a terrain that retains the structure of other units but appears to be embayed by a low albedo material. It can occur near identified chaos terrain or independently, which is why we do not label this unit with the “ch” abbreviation typically associated with chaos (e.g., Greeley et al., 2000; Figueredo and Greeley, 2004; Doggett et al., 2009). This unit could be related to what is referred to as Low Albedo Plains in other texts (Prockter et al., 1999; Prockter and Schenk, 2005).

#### 4.3.2. Subdued ridge unit ( $rts$ )

The subdued ridge unit (Fig. 4(q)) occurs within the chaos terrain, as observed in the high resolution. They have an indistinguishable morphology from the *ridge-and-trough* unit (Section 4.2.1), but consist partially to completely of a low albedo material (e.g., Section 4.3.1).

#### 4.3.3. Discontinuous unit ( $rt_d$ )

Discontinuous chaos (Fig. 4(r)) consists of dissected, variegated albedo ridges that are morphologically similar to more pristine units including *ridge-and-trough* (Section 4.2.1) and *double ridge* (Section 4.1.1). This unit is interpreted to be pieces of pre-existing units, which are isolated or rotated from their original emplacement.

#### 4.3.4. Variegated albedo chaos unit ( $chv$ )

Within the chaos region as observed at high resolution, variegated albedo terrain (Fig. 4(s)) is a hummocky, pockmarked, and rough terrain containing material with a heterogeneous albedo. There are no identifiable remnants of pre-existing structures (as in Section 4.3.3). It is found mostly near, but within, the borders of the chaos terrain.

#### 4.3.5. Chaos, undivided ( $ch_{reg}$ )

Identified as such at the regional resolution because subdivision is difficult at this resolution, chaos terrain (Fig. 4(n)) in this setting includes a combination of what has previously been referred to as platy chaos and knobby chaos (Greeley et al., 2000). Generally, chaos terrain sits at a lower elevation than surrounding terrain but in some cases is elevated (e.g. Schmidt et al., 2011).

Contact with other units in this region varies, but mostly appears gradational at the regional resolution.

### 4.4. Band material

Usually associated with large ( $>10$  km in width) linear to curvilinear landforms occurring in a range of albedos, band material is subdivided here based on texture (e.g., *smooth band* material or *ridged band* material) and internal morphology (e.g., *medial trough band* or *lineated band*). Bands are identified at regional resolution in this case because of their scale ( $>10$  km wide). Only one band is captured in the high-resolution, a *lineated band* (Section 4.4.4), but is initially identified as a plains unit (Section 4.2.3). The implications of this identification are discussed in Section 7.2.6.

#### 4.4.1. Smooth band unit ( $bs_{reg}$ )

Identified at the regional resolution after Figueredo and Greeley (2004), the smooth band unit (Fig. 4(t)) is a low albedo feature made up by a material with roughness unresolvable at the regional resolution and bounded by two distinct ridges. The edges can be linear to curvilinear and sub-parallel to each other. These bands can extend over 100s of km and have a typical width of 10 km, but can be larger, and commonly pinch-out near their termini.

#### 4.4.2. Medial trough band unit ( $bm_{reg}$ )

The medial trough band unit (Fig. 4(u)) is similar in appearance to the smooth band but has a fine lineated texture with a wide central trough which runs lengthwise along the band (Pappalardo et al., 1998b). Around this central trough, the band exhibits a rough symmetry. *Medial trough bands* appear relatively low in topographic relief and they are also typically more narrow than *smooth bands*, only reaching  $\sim 2\text{--}7$  km in width but can be  $\sim 50\text{--}100$  km in length.

#### 4.4.3. Ridged band unit ( $br_{reg}$ )

A ridged band (Fig. 4(v)) consists of a subparallel set of ridges and troughs contained within a linear to curvilinear band. Within the band, ridges and troughs can terminate or bifurcate along their length. These bands are  $\sim 7\text{--}15$  km in width in this region and can be  $>150$  km in length. Differences between a *ridged band* and a *ridge complex* (Section 4.1.2) include scale and ridge spacing; ridges in a *ridged band* appear to be more evenly spaced and equally sized compared to the varying size and spacing of ridges in a *ridge complex*.

#### 4.4.4. Lineated band unit ( $bl_{reg}$ )

A lineated band (Fig. 4(w)) is similar to a ridged band (Section 4.4.3) at regional resolution but exhibits more of a pinch and swell along the individual ridges within the band, especially on the borders. The ridges that make up the borders of the *lineated bands* unit appear to have a braided texture, as they are curvilinear and can pinch and swell, and can cross cut each other.

### 4.5. Other units

Material units not directly associated with Ridges (Section 4.1), Plains (Section 4.2), Chaos (Section 4.3) or Bands (Section 4.4) are here grouped as Other Units. Both of these units are mapped in the high-resolution mosaic geomorphologic map (Fig. 3(B)).

#### 4.5.1. High albedo smooth unit ( $has$ )

Crosscutting all other local units, except for a few prominent fractures, high-albedo mantling material (Fig. 4(y)) appears to overlay and obscures other pre-existing structures or materials. Non-uniform in shape and diffuse in nature, the high-albedo smooth unit is observed in patches with an area of  $\sim 10\text{--}25$  km<sup>2</sup>. There appears to be no spatial correlation with any other unit in the high-resolution images.

#### 4.5.2. Mass wasted material unit ( $mw$ )

The mass wasted material (Fig. 4(z)) identified in the high-resolution images consists of a mostly high albedo material on a slope. There is also an apparent low albedo material distinctly downslope of the higher albedo material and streaks of low albedo material trending downslope. This material occurs adjacent to chaos regions, on *scarps* (Section 5.2.1), and within structural troughs (Section 5.5.2.2).

## 5. Structural map and units

The three major structural units identified in the high-resolution region are Ridges, Troughs, and Craters. We include the *chaos material* (Sections 4.3.1–4.3.4) on the structural map (Fig. 3(C)) in order to highlight the structure, or lack thereof, within the chaos regions. Within this section, we use the term “subdued” to describe structures that do not appear fresh because they have been: (1) severely dissected by other structures, (2) extensively pitted, or (3) have gentler slopes or are topographically diminished in comparison their well-preserved, potentially less degraded, counterparts.

## 5.1. Ridge structures

Here, ridges are sub-divided by their apparent preservation of the original formation structure (e.g., *ridge-and-trough* and *subdued ridge-and-trough*), the number of ridge peaks within the structure (e.g., *double ridge* and *ridge complex*), and insights from the regional resolution (e.g., *band ridge-and-trough*).

### 5.1.1. Ridges-and-trough structures (*rt*)

Ridge-and-trough structures are defined by a systematic sub-parallel ridge-and-trough repeating sequence, which lack the characteristics of being subdued.

### 5.1.2. Subdued ridges-and-trough structures (*rts*)

Subdued ridge-and-trough structures are defined by a systematic subparallel ridge-trough sequence (Section 5.1.1) but appear degraded due to heavy dissection by the post-dating *fine lineations* (Section 5.2.4) structural unit. Additionally, these structures are topographically subdued compared to the well-preserved *ridge-and-trough* structures (Section 5.1.1).

### 5.1.3. Double ridge structures (*dr*)

Double ridge structures are defined by a pair of ridges separated by a single trough, usually containing low-albedo material. These *double ridge* structures are observed to have minimal apparent degradation with smooth slopes and quasi-symmetric ridges. Each ridge is ~300–500 m wide, with heights measured in other works to be 100–300 m (e.g., Head et al., 1999 and Dombard et al., 2013).

### 5.1.4. Subdued double ridge structures (*rds*)

Subdued double ridge structures are identified the same way as well-preserved *double ridge* structures (Section 5.1.3), except in that *subdued double ridge* structures are topographically subdued as well as heavily pitted.

### 5.1.5. Ridge complex structures (*rc*)

Ridge complex structures contain ridges that are topographically higher (>100 m) and individually wider (>500 m) but contain fewer and less regular ridges than a set of *ridge-and-trough* structures (Section 5.1.1). The ridges within a *ridge complex* can range from subparallel to curvilinear with respect to each other and can bifurcate. These *ridge complex* structures appear slightly or not at all subdued.

### 5.1.6. Subdued ridge complex structures (*rcs*)

Subdued ridge complex structures have the same definition as *ridge complex* structures (Section 5.1.5), but have been broadly subdued by pits and dissection. Additionally, *subdued ridge complex* structures have gentler slopes and less prominent topography.

### 5.1.7. Band Ridge-and-Trough structures (*rtb*)

At the regional resolution, a *lineated band* (Section 4.4.4) crosses through the high-resolution region. In the high resolution, this band consists of small-scale (~50–200 m) curvilinear ridges and troughs that appear to be triangular in cross-section.

### 5.1.8. Ropy ridge structures (*rr*)

Ropy ridges are similar structurally to *complex ridges* (*rc*) but are more rounded in cross-section, have gentler slopes, and the overall width of the structure is narrower (<3 km wide). *Ropy ridge* structures are also typically low albedo and are observed to be roughly subparallel. *Ropy ridges* appear relatively well preserved, with little to no evidence of being subdued.

## 5.2. Troughs and associated structures

This structural category contains types of scarps and troughs, and other linear structures with negative topography.

### 5.2.1. Scarp structures (*sc*)

A scarp expressed as a quasi-vertical topographic displacement of a geologic unit or structure. It is identified by where the pre-existing terrain was continuous before the formation of the *scarp* and inferred associated fault. The area between the *scarp* and the presumed fault has been exposed due to the relative motion of the footwall with respect to the hanging wall. The area between the *scarp* and the fault thus probably consists of heavily fractured and mass-wasted material (Section 4.5.2).

### 5.2.2. Trough structure (*t*)

Trough structures generally encompass sharp topographic lows that crosscut pre-existing structures. They do not appear to be associated with other ridge structures and can occur independently or in sets. *Troughs* lack significant raised edges, which differentiate them from ridge types. In general, *troughs* make up the stratigraphically youngest structures on Europa's surface. *Troughs* appear to have steep, near-vertical, sides. They appear to contain a low albedo material, but this could represent shadowing if the slopes are >80°, based on the low incidence angle of the high-resolution images. The typical length of a major *trough* varies from ~4–15 km in this region and have associated widths of ~50–100 m

### 5.2.3. Minor trough (*tm*)

A minor trough is identified by its small size (<50 m in width) or if it is significantly subdued by dissection or shallow topography.

### 5.2.4. Fine lineaments

Not shown in the structural map figure to reduce clutter, but identified in Fig. 6, these linear features are identified by apparent striations or fine troughs (<30 m wide). The fineness and multitude of these structures results in an overall linear trend or texture that transects other observed structures.

## 5.3. Craters (*c<sub>reg</sub>*)

Circular to quasi-circular depressions are identified as pits or craters in the high-resolution images. Because the incidence angle highlights albedo over morphology, it is difficult to see the rim topography and ascertain whether the observed features are truly impact craters, let alone whether they represent primary or secondary impacts. An important note regarding these pits identified in the high-resolution images is their concentration in the eastern portion of the study region. This spatial correlation will be discussed further in Sections 6.6 and 7.1.6.

## 5.4. Materials

These material or morphologic units are included on the structural map for spatial reference, including *high albedo smooth* (*has*, Section 4.5.1) and *chaos* (Section 4.3) units.

## 6. Results: notable morphological and structural mapping observations

In this section, we discuss the observations from the geomorphological and structural mapping of the high-resolution images resulting from comparing the high-resolution and regional resolution geomorphologic maps. The analysis of these observations is in the discussion (Section 7).

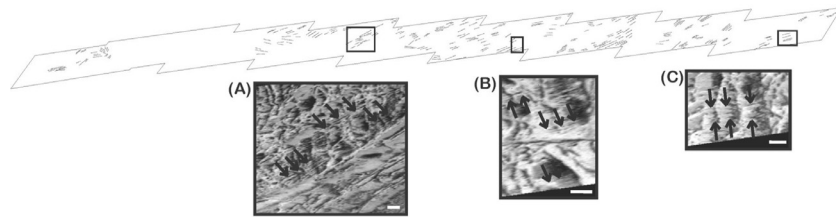


**Fig. 6.** Examples of the *fine lineaments* structural unit defined in Section 5.2.4. Note the possible differences in structural origin. In the bottom left panel, the *fine lineaments* orientation and location suggest a loading origin. In the bottom middle panel the *fine lineaments* are potentially tectonic in origin, related to the formation of the ridges as a tectonic fabric. The *fine lineaments* in the bottom right panel appear independent of the ridge complex it crosses and does not have an apparent loading origin. The *fine lineaments* here also may have accelerated sublimation as we see slight topographic effects on the ridge where the lineations occur. White scale bar in all panels is 500 m.

**Table 2**

Comparison of *subparallel ridge-and-trough* formation mechanisms against observations in the high-resolution mosaic.

	Tilt-Blocks	Folds
Symmetric Ridges		
Systematic		
Shallow Slopes		
Can Bifurcate		
Linear or Curvilinear		

Green indicates where theory satisfies the observation, and red indicates where it is unclear or not satisfied.

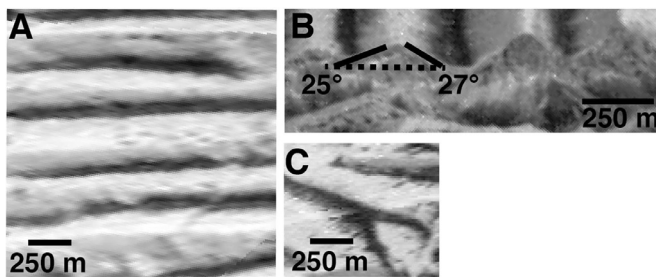


**Fig. 7.** Examples of ridge-and-trough attributes as listed in Table 2. (A) An example portraying the sub-parallel, linear and regularly spaced nature of the ridge-and-trough terrain. (B) A cross-section of the ridge-and-trough terrain displaying the apparent angle of the slopes of the individual ridges (ranging from 20 to 35°). (C) An example of a y-junction or a bifurcating ridge.

### 6.1. Ridge-and-trough systems

Focusing on ridge-and-trough systems (e.g. *subparallel ridge-and-trough* unit, Section 4.2.1), there are four observations which are relevant to potential formation mechanisms from the high-resolution images and the geomorphologic and structural maps: (1) the presence of symmetric, shallow slopes, (2) a curvilinear to sinuous shape of the individual ridges along their length, (3) the presence of ridges bifurcating along their length, and (4) a systematic trend in the orientation of the ridge-and-trough sets (Table 2, Fig. 7). Another notable characteristic includes the relatively consistent widths of individual ridges at 300 +/- 100 m and a width to length ratio of the individual ridges of <0.1. The total width or the length of a ridge-and-trough system is not determinable using these high-resolution images because of the limited extent of the images. The troughs separating each ridge contain a low albedo material, potentially emplaced by ice sublimation or downslope movement (Spencer, 1987).

### 6.2. Double ridges

The observations to especially note of the *double ridges* in this region are: (1) the ability to be generally constant in uniform shape and size along the length of the ridge at this scale (Fig. 8), (2) the range of sizes and scales exhibited (from 500–1200 m in

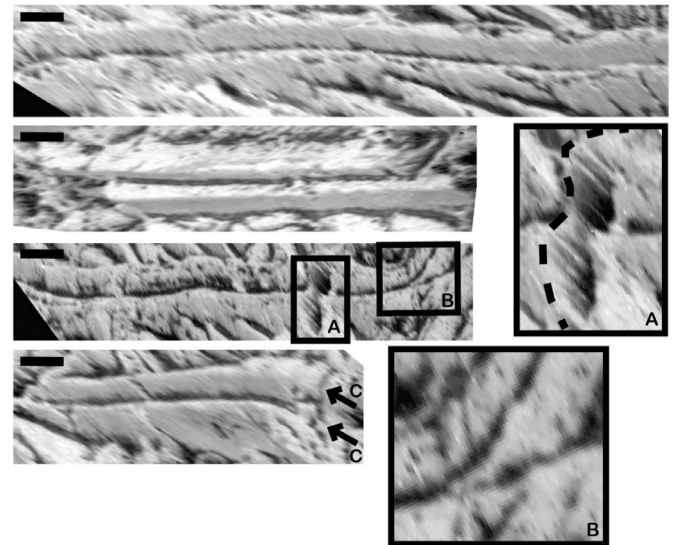


**Fig. 8.** Example of *double ridge* attributes as listed in Table 3. (A) A cross section of *double ridge* reveals that the individual ridges are relatively symmetric. (B) An example in the high-resolution strip of where a *double ridge* evolves along its length into a potential *ridge complex*. (C) In some cases, *double ridges* appear strong and coherent, enough so to be unaffected (in shape) by pre-existing topography and post-formation deformation (second image from top) while in other cases (C, arrow) ridges appear easily fractured across. (D) The only example of a *double ridge* ending without evolving into another feature or being crosscut by newer structures. Scale bars indicate 500 m.

total width in this high-resolution mosaic alone), (3) the symmetric ridges on either side of the central trough (Fig. 8(A)), (4) that a *double ridge* can join or split from a *single ridge* or *ridge complex* (Fig. 8(B)), (5) that *double ridges* can crosscut other units or be crosscut (Fig. 8(C)) indicating these structures have formed throughout the surface history, and (6) that the structures are not significantly affected by any observable pre-existing topography. These observations from the high-resolution images could differentiate among and evaluate the proposed formational mechanisms (Table 3, Fig. 8), which is discussed in detail in Section 7.1.2. In this region, *double ridge* width varies locally from 500–1200 m as seen in this high-resolution mosaic (Fig. 3(A)), similar to previous analyses from other regions (e.g., Head et al., 1999). At the regional or global resolution, this range in widths is considered to be negligible and *double ridge* width is essentially constant (e.g., Greeley et al., 2000). At the high-resolution however, we take this to be a sizeable local variation in width that must be taken into consideration when analyzing potential formation mechanisms.

Though there is only one example in this high-resolution strip, *double ridges* can transform into other feature types along their length, including *ridge complexes*, *ropy ridges*, or *troughs*. It is not surprising that this observation is limited in this high-resolution, given the orientation and limited extent of the images. In this case, the *double ridge* abruptly includes a medial ridge along its length,

**Table 3**  
Comparison of *double ridge* formation mechanisms against observations in the high-resolution mosaic.

	Cryovolcanism	Tidal Squeezing	Linear Diapirism	Shear Heating	Wedging	Compression	Compaction
Uniform height/shape along length	Red	Red	Green	Red	Red	Red	Green
Symmetric Ridges	Red	Red	Green	Green	Green	Green	Green
Small-scale variation in size	Green	Green	Red	Red	Red	Green	Red
Morphs into other structures	Red	Green	Green	Red	Red	Red	Green
Younger or older stratigraphically	Red	Red	Green	Green	Green	Green	Green
Not inhibited by previous topography	Green	Red	Green	Green	Green	Green	Green
No apparent central “crack” or vent	Red	Green	Green	Green	Green	Green	Green

Green indicates where theory satisfies the observation, and red indicates where it is unclear or not satisfied.

**Table 4**  
Comparison of Chaos formation mechanisms against observations in the high-resolution mosaic.

	Melt-Through	Lens	Diapirism
Abrupt Boundaries	Red	Green	Green
Heavily Modified Edges	Red	Green	Green
Preservation of Structures	Green	Green	Green
Low Albedo Smooth material	Green	Green	Red
Lack of large plates	Red	Red	Red
Scale	Green	Green	Green

Green indicates where theory satisfies the observation, and red indicates where it is unclear or not satisfied.

transforming it into a *ridge complex* (Fig. 8(B)). Thus, this ability to transform along its length becomes a requirement for the formation process of a *double ridge*. Additionally, there is one example where a *double ridge* abruptly ends and there is no observed medial fracture (Fig. 8(C)), providing another potential indicator for formation mechanism.

### 6.3. Chaos

There are a few different theories for the formation of chaos terrain (Section 4.3), including: melt-through (Greenberg et al., 1998; O’ Brien et al., 2002), diapirism (Pappalardo et al., 1998a; 1998b; Schenk and Pappalardo, 2004), and melt-water lens collapse (Schmidt et al., 2011; Soderlund et al., 2013). The key aspects of the mapped region are: (1) the abrupt border between chaos and other terrains (Fig. 9(B)), (2) the heavily deformed border regions, (3) the preservation of pre-existing structures (Fig. 9(A), see Sections 4.3.2 and 4.3.3, *subdued* and *discontinuous chaos* terrain, respectively), (4) the presence of a *low albedo smooth* material (Section 4.3.1), (5) the lack of visible plates and likewise, (6) the overall scale of the chaos terrain (Table 4).

### 6.4. High albedo mantling material

The high-resolution images revealed a surface morphology not noted on Europa previously: a relatively smooth, *high-albedo smooth* material (Section 4.5.1) that appears relatively flat and is contained within a small (<1 km<sup>2</sup>) area in multiple locations across the high-resolution region. This unit is inferred to be rough

at a smaller scale than the image resolution. This material is pitted and appears to subdue crosscutting structures (Fig. 10).

### 6.5. Small pits and craters

One of the features unmarked in the structural map considering their number (>1700) and unrecognized in the regional resolution due to their size (30–75 m in diameter) are the small pits and craters (Fig. 11). These pits and craters are quasi-circular structural features that tend to be high albedo at the rim and contain low albedo material within a bowl-shaped depression.

### 6.6. Fine lineaments

Another observation revealed only by this high-resolution and detailed mapping is the pervasive linear feature trending N75E–N81E. This feature was not included on the structural map to avoid clutter (Fig. 3(C)), but when observed alone (Fig. 6) it is evident that these *fine lineaments* (Section 5.2.4) are pervasive across the high-resolution image. Additionally, these structures are not parallel to the image projection (or elongation of the pixels) and change direction slightly across the mosaic, indicating that these features are not an artifact of image processing. In the images, the *fine lineaments* consist of spatially grouped (~50 m spacing), thin fractures or troughs. Particular features in this class appear to be related to prominent structures (Fig. 6(A)), while others appear to be related to slopes or mass wasting of topographically high structures (Fig. 6(B)), whereas others still appear to be unaffected by the

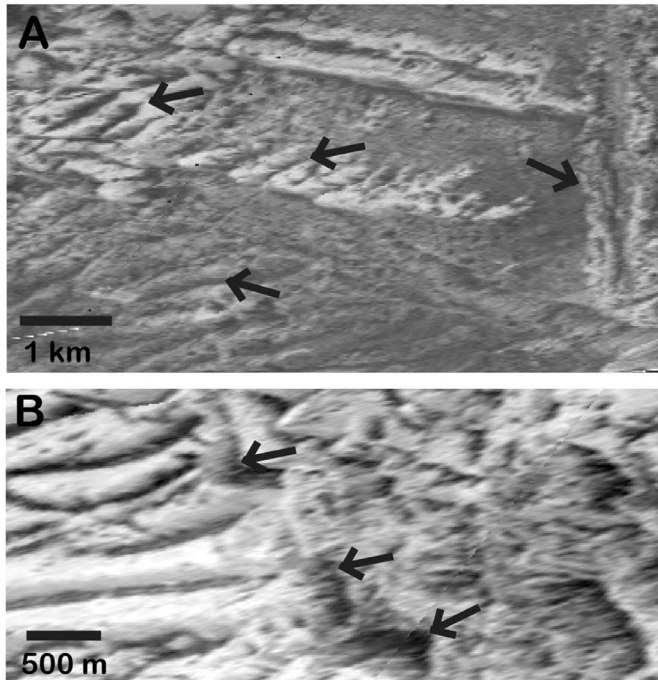


**Fig. 9.** Examples of chaos attributes as listed in Table 4. (A) Surviving structures in chaos region. The red box indicates a slightly modified but mostly intact *double ridge*. Arrows indicate part of what is interpreted to be a *ridge-and-trough* and *double ridge* unit completely embayed by the *low albedo smooth* material (see Section 4.3.1). The preservation of these units has implications for chaos formation, as the mechanism must allow for embayment and mild modification in addition to the heavy modification of other nearby units. (B) The sharp boundary between well-preserved ridged-trough terrain and chaos terrain. North is up.

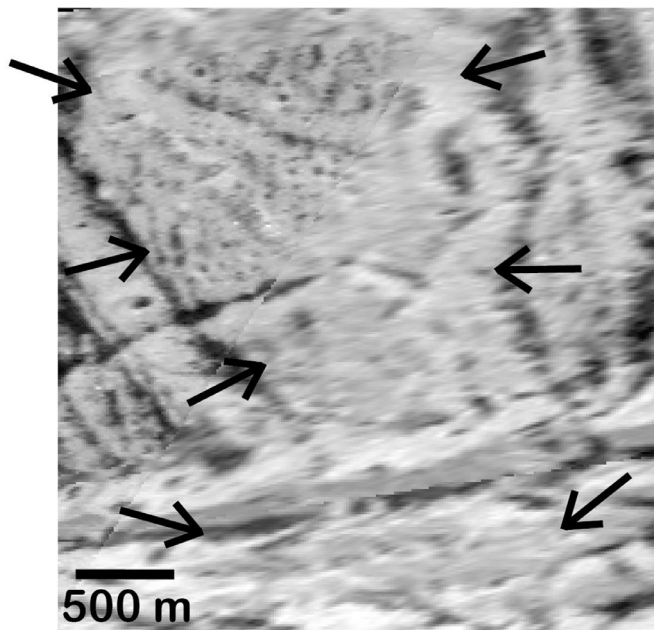


**Fig. 10.** The arrows denote the edges of the *high albedo smooth* material. Note how the features around the high albedo region have troughs and ridges, but the area within the arrows consists mostly of small (~10 m) pits, subdued troughs and smooth material. This material also appears to have degraded the *subparallel ridge-and-troughs* at the bottom of the image.

presence of these prominent structures at all and simply crosscut them (Fig. 6(C)).

### 6.7. Comparison between high-resolution and regional resolution maps

Unsurprisingly, there are a few clear differences between the regional resolution image and the high-resolution images. What is unexpected is that these differences go beyond simply greater detail and the enhanced ability to discern different morphologies. These noted differences include: (1) potential surface changes, (2) misidentification of chaos terrain, and (3) constraints for the formation of morphologically different bands. Each of these noted observations are explored in detail in Section 7.2. In particular cases, the differences in the high-resolution images provide caution for maps at regional resolution and can help us understand how certain features form.

## 7. Discussion

Herein, we evaluate the observations from the high-resolution mapping (see Section 6) using previously proposed formation hypotheses, or our own hypotheses as appropriate.

### 7.1. Surface feature formation mechanisms

The E12 Mottle high-resolution region is structurally intricate and tectonically complex. While we cannot unravel its entire surface history considering the limited extent of the high-resolution strip, there are multiple observations gained from the mapping that will aid in constraining formation mechanisms and relative ages of different structures. In this section, we will address whether our observations (Section 6) agree or disagree with observations made from the regional resolution mapping or from predictions made by different formation models for a variety of structures and materials, including: *ridge-and-trough*, *double ridges*, *chaos*, *high albedo smooth*, *craters*, and *fine lineaments*.

#### 7.1.1. Ridged plains

As stated in the unit description, not much is certain about the ridged plains or ridge-and-trough material, besides that it can appear in various different forms or sub-units in the highest resolution images (Head et al., 1999; Patel et al., 1999a; 1999b; Kattenhorn, 2002). The existing proposed formation mechanism, specifically for the subunit of *subparallel ridge-and-trough* material, is a type of normal faulting that would produce tilt-blocks (Kattenhorn, 2002), akin to the grooved terrain on Ganymede (Pappalardo and Greeley, 1995; Prockter et al., 1999, 2000; Figueredo and Greeley, 2000). However, a high-resolution analysis of Europa's ridge-and-trough terrain has not been performed prior to this work. The tilt-block hypothesis likely does not support most of our observations from the high-resolution region (Section 6.1, Table 2). If the ridge-and-trough systems were formed via an extensional tilt-block mechanism, the ridges would not bifurcate as commonly observed in the high-resolution images (Fig. 7(C), Table 2, Pappalardo and Greeley, 1995; Head et al., 1998; Leonard et al., 2015). The slopes of the individual ridges in the ridge-and-trough systems are relatively symmetric in cross-section, additionally indicating that the tilt-block mechanism is likely not the formation mechanism for ridge-and-trough terrain as this would preferentially produce asymmetric slopes, with only a special case producing symmetric ridges (Fig. 7(A) and (B), Pappalardo and Greeley, 1995; Kattenhorn, 2002; Leonard et al., 2015). In order to produce a symmetric cross-section, the slopes of a tilt block must be ~45°, which is not observed and neither is the necessary mass-wasting to make the slopes shallower (Fig. 7(B)).

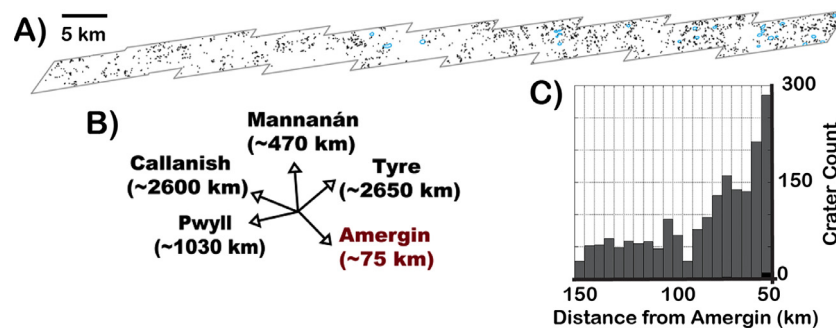


**Fig. 11.** (A) Map of each small pit (black dot) and dark spot (light blue) in the high-resolution image. North is up. (B) An indication of the closest or largest primary craters on Europa and their distances to this region. (C) Plot of number of pits (grey) and spots (black) with increasing distances from Amergin, the closest primary crater. Note the exponential fall off thus indicating that these spots are likely secondary craters. (For interpretation of the references to color in this figure legend, the reader is referred to the web version of this article.)

If the *subparallel ridge-and-trough* terrain formed via a compressional folding mechanism, as proposed in Head et al. (1999) and explored by Leonard et al. (2015), the observed characteristics could be produced. Folds allow for slopes ranging from symmetric to asymmetric, with no particular preference. Additionally, the slopes of folds are dependent on the amount of applied stress to some extent, and therefore can be anywhere from shallow, like we observe (Fig. 7(B)), to quasi-vertical, or isoclinal. Folding can also create ridges that bifurcate along their length (Leonard et al., 2015). Thus, we conclude that a folding mechanism best fits the observed characteristics of the *subparallel ridge-and-trough* structure and morphology of ridged plains in this region. This could be the case for the other ridged plains morphologies, but we do not have cross-sectional information for *convex*, *hummocky*, or *mélange ridge-and troughs*, so we verify cannot verify this hypothesis for those units.

### 7.1.2. Double ridges

There are multiple hypothetical models for the formation of *double ridge* structures including cryovolcanism (Fagents and Greeley, 1997; Kadel et al., 1998), tidal squeezing (Greenberg et al., 1998), linear diapirism (Head et al., 1999), shear heating (Nimmo and Gaidos, 2002), compression (Sullivan et al., 1998), wedging (Melosh and Turtle, 2004; Han and Melosh, 2010; Johnston and Montési, 2014), and compaction (Aydin, 2006). We compare these different hypotheses to our observations from the high-resolution mapping (Section 6.2, Table 3, and Fig. 8).

Cryovolcanism, as proposed by Kadel et al. (1998), requires repeated or continuous expulsion of material from below the surface along a central trough vent such that the material piles up on either side to form the ridges. Cryovolcanism could take place in an explosive or effusive manner (Fagents, 2003). While this model explains the local variation in size and shape of the *double ridges* fairly well, it is difficult to explain how the majority of observed *double ridges* would end up fairly uniform in width and height along their length (Fig. 8). Cryovolcanism is likely an intermittent process along a series of trough vents that would lead to irregular *double ridges* that pinch and swell more often than observed in the high-resolution images. Flanking fractures associated with *double ridges* are not observed in this region and thus cannot be used to support cryovolcanism as the primary mechanism for forming *double ridges* (Dombard et al., 2013). As such, cryovolcanism as a formation mechanism for *double ridges* is unlikely as it cannot produce symmetric (Fig. 8(A)) and regionally consistent structures with only small-scale variations.

The tidal squeezing model involves a fracture opening and closing repeatedly from the effects of diurnal stresses generated as the satellite travels its slightly eccentric orbit around Jupiter. When the crack opens, water from below or warm ice flows up

to the surface; when the crack closes, the material is pushed up to form the flanking ridges (Greenberg et al., 1998). However, the mechanism for the fluid or slush to reach the surface is tentative (Crawford and Stevenson, 1988) and whether or not diurnal stresses would have the ability to crack the ice shell is unclear (Greenberg and Geissler, 2002). Additionally, like the cryovolcanism hypothesis, the tidal forces and the amount of material squeezed out would not remain constant along the *double ridge* and spread evenly to both sides, especially with observed pre-existing topography present (Fig. 8(A)). One of the appealing aspects of this model is that it could explain how one type of ridge might transition into another along its length (Fig. 8(B), Geissler et al., 1998). For example, if the crack was closed, it might appear to be similar in structure to a *single ridge* or if, in response to the changing nature of the surface stresses, a *double ridge* underwent only extensional stress for a time, the ridge might widen to form a *ridge complex*. However, the small-scale variation in size of the *double ridges* that we observe is also not well explained by this model, as it appears the ridges would continue to grow for as long as the stress conditions allowed, leading to significant variations in size not observed in the high-resolution images. Overall, these first two hypothesized methods of formation have similar problems because they involve a mobile material rising and extruding directly onto the surface likely causing width and height variations along the length of the ridge (Fig. 8), but such is not observed.

Linear diapirism, a model proposed by Head et al., (1999), is related to the sparse examples of linear diapirism that takes place in Earth's crust. On Europa, the authors propose that an initial crack is formed by tidal stresses and a buoyant, ductile material exploits this weakness in the brittle upper crust and upwells. This upwelling pushes the brittle crust up around the linear diapir forming the two symmetric ridges of the *double ridge* (Head et al., 1999). Though it is debated whether this mechanism would be able to produce such a linear ridge (Greenberg et al., 1998), the size of the ridge would relate to the size of the diapir and the thickness of the lithosphere, making the *double ridges* potentially consistent in size (Fig. 8). Linear diapirism would not be affected by pre-existing topography, only depending on where the ice shell was weakest. Additionally, this would allow for preservation of pre-existing terrain observed on a few ridge flanks (Pappalardo et al., 1998b; Greenberg and Sak, 2014), even though we do not observe this feature in this high-resolution region. The greatest weakness of this hypothesis is that this mechanism might not produce the relative regularity in width and height of a *double ridge* along its length and there is no definitive example on Earth to demonstrate this model (Fig. 8(A)).

Similar to the idea that heated ice would cause an upwelling or upwarping of the brittle top layer, Nimmo et al. (2002) propose that tidally forced movement along a strike-slip fault would

cause an upwarping and, if melting occurs, a collapse of the center, which would form the *double ridge*. The linearity of the feature in this case is due to the idea that a *double ridge* is a strike-slip fault created by tidal stress, as opposed to the melt-water lens collapse hypothesis that is proposed to form chaos terrain (see Section 7.1.3). The heating and upwarping could result in symmetric ridges as long as physical properties of the ice shell were locally constant (e.g., prominent structural obstacles or changes in material properties). However, the shear heating mechanism proposed by Nimmo et al. (2002) is unlikely to produce enough heat to produce the observed features (Han and Showman, 2008). The process could potentially preserve the pre-existing topography or cover it with mass wasting. The size and shape of the *double ridges* in this model would relate to the magnitude of the stress acting on the particular ridge, bringing into question whether a consistent width ridge along its length could be produced (Fig. 8).

The wedging model, similar to linear diapirism, involves material rising from the subsurface but unlike linear diapirism, this material does not reach the surface in the wedging model. If a linear liquid water dike forms underneath the European surface, Melosh and Turtle (2004) argue that the imposed stresses could create a *double ridge* on the surface, supported by the later work of Han and Melosh (2010). However, modeling performed by Johnston and Montési (2014) concluded that the circumstances for this model to work and match the observed structure of a *double ridge* were unlikely at best due to size limitations. Thus, most likely, the wedging model cannot reproduce the size or consistent shape we observe (Johnston and Montési, 2017).

Sullivan et al. (1998) suggest that the formation of a *double ridge* would occur when a fracture opens and then is compressed together repeatedly to cause the area around it to bulge upward. This model is attractive, given that there is a lack of identified contractional features to match the proposed extensional features on the European surface (Prockter and Pappalardo, 2000; Sullivan et al., 1998; Prockter et al., 2002). However, compression does not explain how *double ridges* can transform along their length into other features like bands or *ridge complexes* (Fig. 8(B)), with the exception of *single ridges*. The symmetry of each ridge is also unlikely in a compressive stress field with a brittle material, where it is more likely that one side would dominate (as in the case of thrusting on Earth) instead of being relatively equal. The idea that *double ridges* could accommodate some of the missing surface contraction on Europa does not end with Sullivan's compression model (Aydin, 2006; Culha et al., 2014), and while there is observational support (e.g., Patterson et al., 2006; Kattenhorn and Prockter, 2014), it is not present in these high-resolution images.

The compaction band model, proposed by Aydin (2006), requires the *double ridges* to have formed by localized strain where a porous material is compressed. Because the porosity of the surface materials is not well constrained and could vary greatly in space and time, owing to variations in surface history, this mechanism may have operated at a local scale and particular time of *double ridge* evolution. Assuming the surface materials have the necessary properties, Aydin's model provides a medium to allow contractional surface features with the needed symmetry and theoretical ability to develop into other features (Aydin, 2006). In the high-resolution images however, the *double ridges* are rounded in cross-section and have gentle flanking slopes (Fig. 8(A)), whereas the Earth analog examples provided by Aydin (2006) display steeper ridge limbs and rounded ridge tops. Thus, in order for compaction to form the *double ridges*, the slopes must have mass wasted or viscously relaxed to make their slopes shallower, an unlikely mechanism because viscous relaxation preferentially degrades long-wavelength features. We see no direct evidence for mass wasting along the *double ridge* flanks in the high-resolution images, but it has been observed in association with *double ridges* in other re-

gions (e.g., Head et al., 1999; Spaun et al., 2003). Nonetheless, this model succeeds where most others do not, in creating a viable mechanism for producing symmetric and consistently sized *double ridges* across the surface.

The observations from the high-resolution images, particularly the consistent and symmetric ridge morphology, and the ability to be unaffected by previous topography, reveal strengths and weaknesses in all the current formation theories. The high-resolution images cause us to place emphasis on symmetry and consistency for *double ridge* formation, leading us to interpret that linear diapirism and compaction are best fit to the observations. Because these hypotheses do still contain weaknesses, it is important to consider the possibility that a combination of processes could be at work to form the *double ridges*, or that there is a completely different process producing *double ridges*.

### 7.1.3. Chaos

There are multiple hypothetical models for the formation of chaos regions, including: melt-through (Greenberg et al., 1999; O'Brien, 2002), diapirism (Pappalardo et al., 1998a; 1998b; Schenk and Pappalardo, 2004), and the collapse of a melt-lens within the ice shell (Schmidt et al., 2011; Soderlund et al., 2013). We compare these different hypotheses to our observations from the high-resolution mapping (Table 4 and Fig. 9).

The melt-through model of chaos formation involves direct contact, or melt-through, of the underlying ocean with the surface of the ice shell. This melting is suggested to take place over time as tidal heating occurs in the subsurface ocean and within the ice shell. This model requires a thin ice shell in order for the heat flux required to produce the melt-through of the ocean to be reasonable for Europa (Greenberg et al., 1999; O'Brien et al., 2002) and for the ice shell to resist rapid flow which would prevent melt-through (O'Brien et al., 2002). The idea of a thin-shell (<5 km) in general is not favored for the present epoch, considering the numerous lines of evidence indicating the presence of a thicker shell (e.g., Pappalardo et al., 1999; Prockter et al., 1999; Schenk, 2002; Nimmo et al., 2003; Figueredo and Greeley, 2004; Prockter and Schenk, 2005). The melt-through model of chaos terrain formation predicts a down-sloping "beach" (Greenberg et al., 1999) rather than the abrupt boundary of the chaos unit observed in the high-resolution images (Table 4). The model also predicts features just outside of the chaos region, especially ridges, to sit upon a relatively thicker shell and withstand the melting and chaos formation. There are no peninsulas or such formations in the high-resolution chaos, but there are preserved features within the chaos that might have withstood the melting preferentially (Fig. 9(A)). Thus, the melt-through model could potentially explain the apparent embayment of pre-existing and preserved structural features in the chaos region. The Greenberg et al. (1999) model explains the variation in sizes of chaos terrain by the limited heat flow in the specific region. The region of chaos directly to the west of the high-resolution region (Fig. 2) could help contribute to smaller areas of thinning in neighboring areas. While a few of the observations fit fairly well, the transition from other terrain to the chaos terrain does not, and it is unclear how this mechanism could produce the amount of tectonic modification observed within the chaos region.

The melt-water lens collapse model proposes that as thermal activity causes ice to melt (in response to impacts, shear heating, or endogenic heat sources), melt water lenses form. These lenses are sealed off from their surroundings and therefore cause a downwarping of the surface due to volume conservation. The subsequent collapse of these pressurized lenses is suggested to be responsible for the chaos terrain (Schmidt et al., 2011; Soderlund et al., 2013). During collapse of the lens, it is suggested that volume could be injected through fractures that when refrozen and volume

increases, would cause an upwarping in the area. Thus, depending on where the chaos region is in its development, it could be topographically high or low (Michaut and Manga, 2014). Differential water injection and refreezing within the chaos region lends itself well to the variety of topographic features in the high-resolution chaos region and could possibly explain why some units appear flooded, or embayed, with a low albedo material. This model could explain the observed heavily modified terrain near the edges of the chaos region, as due to episodes of downward warping and upward warping as the lens forms, then collapses, and finally refreezes (Fig. 9(B)). A new observation from the high-resolution images is the preserved structures within the chaos region. Though embayed features have been inferred previously (e.g., Carr et al., 1998; Prockter and Schenk, 2005), they are outside of the deformed chaos terrain or on floating or tilted blocks. The structures we observe in this region are completely embayed, but the basic structures are still preserved, and are well within the broken-up border regions of the chaos terrain. The melt-water lens collapse hypothesis fits this observation, as the center of the chaos region could potentially be one of the better-preserved areas in this model (Fig. 9(A)).

Chemically or thermally driven solid-state diapirism has also been suggested as a possible model for the chaos terrain formation. Convective diapirs are proposed to transport tidal heat produced deep in the ice shell to the surface (Pappalardo et al., 1998a). When the diapir rises underneath the brittle portion of the ice shell it first upwarps the ice, potentially hundreds of meters (Pappalardo and Barr, 2004), before possibly down-warping if there is extrusion or collapse (Schenk and Pappalardo, 2004). In this region, the latter would be the case because the topography is depressed compared to the surroundings (Fig. 9(B)). The heavily modified edges of the chaos in the high-resolution images agree with this model because this is where the topographic changes would be breaking up material, while the middle would contain sections that could potentially be more preserved (Fig. 9(A)). Extrusion around the edges of the chaos region might explain the *low albedo smooth* material, but it is not clear whether this could cause the material that we see embaying units near the center of the chaos region, especially because it is not a topographic low.

With respect to the high-resolution observations, none of the chaos formation models are a perfect fit. Each has observations that agree and potentially disagree with the high-resolution mapping such as degree of modification, placement of modification, or the presence of a low albedo material (Table 4). The abrupt and heavily modified boundaries of the chaos region and the preserved structures are the defining features in the high-resolution images and therefore the observations in the high resolution favor the melt-water lens collapse hypothesis. It is unclear whether any of the models allow for a lack of broken-up plates within the chaos region. Thus, more high-resolution data in other chaos regions is necessary to make observations and determine the role of platy chaos versus the knobby texture and preserved, but embayed, structures we observe in this high-resolution region.

#### 7.1.4. High albedo smooth material

The high albedo material (Fig. 10) on Europa has not been discussed or analyzed before. There are a few potential possibilities for the origin of this material: (1) emplacement by a cryovolcanic or frosting process, (2) destruction of structures by secondary impact or other impact process, or (3) it is a terrain that is shaped by processes resolvable only below the scale of these high-resolution images.

The first mechanism that we suggest for the creation of the *high albedo smooth* terrain is the possibility of an overlain high-albedo material, potentially covering whatever pre-existing structures might have been present. Because we do not know the na-

ture of the structures that might have predated this terrain, we cannot analyze how much overlying material would be required to cover the pre-existing terrain. In terms of the plausibility of this process however, we can assess the two potential mechanisms for depositing material on top of the surface, cryovolcanism and thermal migration. In order for mantling to occur via cryovolcanic deposits, we would expect to observe a potential source vent, which we do not. This overlain material could also be from a frosting process, which is suggested to occur on colder surfaces which are topographically higher and have higher albedo on Europa (Spencer, 1987). This process is akin to water-ice thermal migration which is proposed to occur on the Moon and Mercury (e.g., Vasavada, 1999). However, there is no observational evidence indicating that this region is standing topographically high compared to the surrounding regions. Without further data, topographic or thermal, we cannot comment further on the plausibility of this process.

Another possibility for the formation of this terrain involves effectively destroying potential pre-existing structures by impacting the terrain, either a primary impact or many secondary impacts. A primary impact is unlikely as this terrain is morphologically unlike any observed craters on Europa (Schenk and Turtle, 2009). Secondary craters tend to occur in groups (e.g., Bierhaus et al., 2001) and have the potential to destroy terrain (see Section 7.2.2). However, this terrain occurs in relatively small (<1 km<sup>2</sup>), uniform regions with abrupt transitions to other terrain types, suggesting that the secondary impacts is unlikely.

When Europa was first mapped using Voyager data, the rough terrain of the ridged plains that we observe in the high-resolution images was identified simply as “plains,” implying a smooth terrain (Lucchitta and Soderblom, 1982). Likewise, when mapping the regional resolution images (>200 m/pixel) on Europa, it is unclear that a terrain like the ridged plains would be present in all the seemingly smooth high albedo regions. As such, the high albedo unit (*has*, Section 4.5.1) we mapped based on the high-resolution images may disguise even finer scale structures, which could be resolved with higher resolution data from future missions such as the Europa Clipper mission.

Without further information, we cannot reliably differentiate among these three possibilities for the formation of this *high albedo smooth* terrain. Nonetheless, this terrain deserves note because of its comparable smoothness to other “smooth” terrains on Europa (Prockter and Schenk, 2005), potentially relevant to landing sites for a possible future lander mission (2016 Europa Lander Science Definition Team Report).

#### 7.1.5. Small pits and craters

We mapped the location of each of the small (<100 m diameter) pits across the high-resolution mosaic, ~1700 in total (Fig. 11(A)). To account for the size and ubiquity of the small pits, the mapping was performed twice in some frames to verify consistency in what was being marked as a small pit. Overall, it is evident that these features are quite abundant (Fig. 11(A)). The three possible formation mechanisms we propose for these small pits are: (1) devolatilization or sublimation, (2) regolith drainage or pit chains, and (3) secondary craters.

Devolatilization or sublimation pits are hypothesized to form in association with recently overturned or uncovered material containing volatiles that then, potentially violently, degas. Because this hypothesis involves material that is overturned or uncovered quickly, devolatilization pits are typically associated with impact craters and ejecta or mass wasting (e.g., Moore et al., 2009). To date, such pits have been identified on Mars, Mercury, Vesta, comets such as 67P, and Pluto (e.g., Gillis-Davis et al., 2009; Boyce et al., 2012; Denevi et al., 2012; Tornabene et al., 2012; Vincent et al., 2015; Moore et al., 2017). On Mars, the pits range from 10 m

to 3 km in diameter (Tornabene et al., 2012) and the pits we observe on are Europa within this range. However, the pits observed on Mars can range in shape from circular to polygonal (Boyce et al., 2012), whereas we only observe these small pits on Europa to be relatively circular. While this shape difference could be an effect of viewing geometry or image resolution (image resolution on Mars is at least 5 times better at  $\sim 3$  m/pixel), it could also indicate a different formation mechanism. Additionally, the small pits we observe in the high-resolution images are not associated with any mass wasting or other obviously overturned material (see Fig. 11(A)), and there is no observational evidence for heating across this entire region that could have potentially released volatiles. Thus, the origin of these small pits on Europa as devolatilization pits is unlikely.

Another potential formation mechanism for the small pits is regolith drainage pits or pit chains. Different from a catena, pit chains are typically associated with extensional faults that are overlain by a regolith or quasi-cohesionless material that drains into the subsurface void. Pit chain formation has been identified on terrestrial bodies, including Earth (e.g., Okubo and Martel, 1998; Ferrill et al., 2011), Moon (e.g., Watters et al., 2012), Phobos (e.g., Thomas et al., 1979), and Mars (e.g., Banerdt et al., 1992; Wyrick et al., 2004), as well as on icy satellites such as Enceladus (Martin et al., 2017). As implied by the name however, pit chains are aligned with each other and can merge to form a quasi-linear structure. The small pits that we observe on Europa do not align in this fashion, but instead they appear in a more random distribution (Fig. 11(A)) and thus are unlikely to form via this mechanism.

Our favored hypothesis is that these features are secondary craters because of their clear increase in abundance with proximity to the 17 km diameter crater, Amergin (Fig. 11(B)). There is limited information regarding secondary cratering on icy satellites, but it is predicted that secondaries dominate the population of smaller (<100 m diameter) surface craters on Europa (Bierhaus et al., 2001, 2005; McEwen and Bierhaus, 2006). The suggested primary crater for the secondaries in this region, Amergin, is located off the southeast corner of the regional image, about 75 km from the center of the high-resolution mosaic. We find that the number of small pits falls off exponentially (Fig. 11(C)) with distance from Amergin, indicating that these pits are secondary craters originating from the Amergin impact.

Two dips in the spatial distribution of small pits occur where chaos terrain dominates the high-resolution image mosaic (Fig. 11(C)). While this could indicate that these chaos regions are younger or have been modified since the primary impact, it is quite plausible that the secondary impacts are more difficult to recognize in the already disrupted, lower albedo material as opposed to the more pristine, high albedo material. Alternatively, it is possible that the material properties of the chaos regions may be responsible for degrading or relaxing the secondary craters to the point where they are no longer recognizable.

The identification of such numerous secondary craters has implications for impact physics on icy satellites. Additionally, the immense range of these secondary craters could be responsible for spreading material over large distances (100s of km) across the surface. This may have important implications for spreading radiation processed oxidants, of importance to potential subsurface biology when the surface is recycled (Kadel et al., 1998).

#### 7.1.6. Fine lineaments

The origin of these pervasive *fine lineaments* is unclear (Fig. 6). There appear to be potentially three types: (1) those related to prominent structures, (2) those associated with slopes or mass wasting of prominent, topographically high structures, and (3) those unassociated with other structures.

The *fine lineaments* we observe that appear to be associated with prominent structures, such as those that run sub-parallel to ridge complexes (Fig. 6(A)), could have formed as a result of lithospheric loading (e.g., Hurford et al., 2005; Collins et al., 2009). This mechanism involves: (1) the formation of the prominent *ridge complex*, causing (2) the lithosphere to flex due to the load of this structure, and eventually (3) cracking to form the *fine lineaments*. Topographic data to find evidence for the potential flexure in the lithosphere could confirm this hypothesis.

The lineaments that are quasi-perpendicular to the trend of other prominent structures and sub-parallel to the slope of these structures, such as the lineaments associated with the *double ridge* in Fig. 6(B), could be formed by mass wasting of a low albedo material. In this case, the lineaments would not be fine cracks, but surficial deposits that mimic fine fractures.

The third proposed type of *fine lineaments*, which crosscut prominent structures and have affected the cross-section of that structure (see Fig. 6(C)), we hypothesize could be the expression of a tectonic fabric. “Fabric” is a term employed in structural geology to describe a linear organization within a rock, usually referring to alignment of minerals or crystals. Here, we use it to describe a relatively consistent, subparallel linear feature within the icy surface. On Earth, fabric in a rock can form by a range of processes and at variable scales. We note that the *fine lineaments* on Europa appears to be planar, another feature of a tectonic fabric, due to its representation by joints or cracks. This implies that this fabric most likely originated from strain (referring to cleavage or foliation) and possibly related to the platy shape of large (meter-size) ice grains (e.g., Schmidt and Dahl-Jensen, 2003). This formation mechanism would imply that the lineaments are the result of a tectonic fabric formed in Europa’s ice over potentially millions to >100s of millions of years of tectonic deformation. The previously described surficial deposit-related *fine lineaments* could also originate as a fabric that causes the change in albedo. Overall, we predict that tectonic fabric should become apparent across Europa once image resolution improves with the Europa Clipper Mission. Additionally, fabrics that include differences in grain size, crystal structure, and apparent albedo could be responsible for roughness on small scales, due to differential sublimation or other weathering effects (Fig. 6(C)).

## 7.2. Regional resolution comparison

We compare the regional resolution geomorphologic mapping (Fig. 2(B)) to the high-resolution geomorphologic mapping (Fig. 3(B)), in order to identify discrepancies when mapping at the more spatially extensive regional resolution (200+ m/pixel). We include the analysis of a possible effect of varying emission angle, a region that appeared to be chaos at regional resolution and plains in the high-resolution, and insights into band formation.

### 7.2.1. Viewing geometry effects

When comparing the regional map (Fig. 2(B)) with the high-resolution structural map (Fig. 3(C)) we notice that a feature present in the regional resolution image does not seem to appear in the high resolution (Fig. 12(A)). Thus, there are two possible explanations: (1) the apparent change is an artifact of different viewing angles (emission angles) and lighting (incidence angles) or (2) it is an actual change in the surface.

The first explanation is more likely; the differences in lighting and observation angle between the regional and high-resolution images are extreme (cf., Malin and Pieri, 1986). The *ridge complex* that the fracture apparently crosses through could be hiding the feature in the high emission angle of the high resolution; the surrounding chaos could be similar to the albedo of the fracture

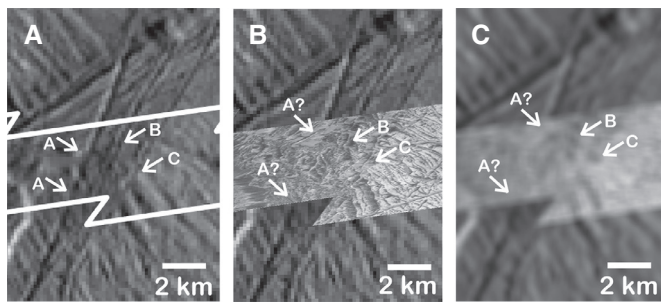


**Fig. 12.** (A) Denotes the ridge observed in the regional resolution image (left) that appears to disappear in the high-resolution image (middle). (B) and (C) denote two other ridges of similar orientation to ridge (A) in the regional resolution (left) that are still observed in the high-resolution images (middle). Note that when the high-resolution image is resampled to approximately match the resolution of the regional image (right), the ridges (B) and (C) are again visible, but the ridge (A) is still not visible. The high albedo feature near the top (A, middle and right) appears to be the ridge complex trending NE and not the ridge (A), as it trends ~N. This is reinforced by the lack of structure at the bottom of the images (A, middle and right).

or could also be hiding the walls of the fracture from observation. The issue with this explanation is that other, directly adjacent and similarly oriented fractures are visible in both the regional and high resolution (Fig. 12(B) and (C)). Additionally, the fracture that appears to have changed is the most prominent of the surrounding fractures (Fig. 12(A)). Despite the size and orientation of ridge A compared to B and C (Fig. 12), we suspect that this discrepancy is explained by the substantial difference in viewing geometry (~60°). This is important to note because the planned Europa Clipper mission is a flyby mission, meaning the images from this mission will have a wide variety of emission and incidence angles, making this an example of the type of discrepancies we might find.

If it were the case that this feature is an indication of surface change, it would not necessarily imply that there is active resurfacing on Europa. For instance, the change in the surface could be a result of mass wasting at that scale; perhaps the fracture was partially filled in by material from the ridge complex or chaos and therefore is no longer visible in this particular region. This idea appears plausible especially given the short amount of time passed (~2 months) between when the Galileo SSI captures the two images and any other change would greatly exceed resurfacing rate predicted by Phillips et al. (2000) of <1 km<sup>2</sup>/year. Whether the feature is an indication of surface change or an artifact of differing observation conditions, it would be interesting to investigate further to see if these types of small-scale changes occur elsewhere when more high-resolution data is made available by the Europa Clipper mission.

### 7.2.2. Misidentified chaos terrain

Mapping chaos regions at regional resolution matches the units mapped in the high-resolution images with one exception, the mapping of a chaos unit at regional resolution that is not mapped as a chaos unit at the high resolution. This area is located at the easternmost frame of the high-resolution (Fig. 13). In the regional resolution, this terrain closely matches other knobby chaos material, but in the high resolution is clearly different and closely matches the plains terrain morphology.

It is evident that this region may have been undergoing a form of morphological modification. The preponderance of small (30–75 m in diameter), dark, quasi-circular features and larger (100–300 m in diameter) dark spots in this region may have led to this misidentification (Fig. 11(A)). The possibility that these dark features are secondary craters is explored in Section 7.1.5. Because we conclude that the small pits are most likely secondary craters, this leads to the idea that chaos identified at the regional resolution

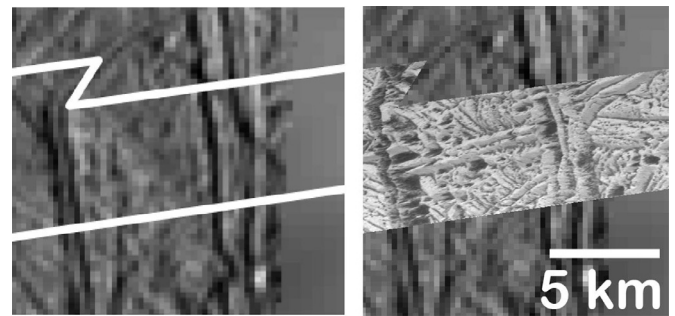


**Fig. 13.** This region is identified as chaos at the regional scale (left), but in the high-resolution image (right), we can see that it does not resemble chaos terrain, but instead, the terrain appears to be modified by a different process. We interpret that this region has been modified by secondary craters (see Fig. 11), even though it is near other chaos terrain. Common scale, North is up.

might actually be modified by secondary cratering. Thus, we suggest that secondary cratering, within 50 km of the primary crater, could have aided in resurfacing by destroying pre-existing structures. Given that there are ~20 observed craters on the surface of Europa of the same approximate size or larger than Amergin (Schenk and Turtle, 2009), and taking a conservative estimate of 50 km radius around the primary, secondary craters would be responsible for altering ~0.5% of the surface to the level observed in Fig. 13. Thus, while this process evidently is not the main contributor to Europa's resurfacing, it could provide a supplement and aid in destroying pre-existing structures, especially when viewed at a small scale.

### 7.2.3. Smooth band formation

The most prevalent hypothesis for the formation of smooth bands involves fracture initiation followed by extension and infilling similar to the formation of mid-ocean ridges on Earth (Prockter et al., 2002). Smooth bands have also been often associated with movement, primarily extension and slip, by matching terminated features on either side of the band (Sullivan et al., 1998; Prockter et al., 2002). Whether these bands can also accommodate contractional movement is still up for debate (Figueredo and Greeley, 2000). The smooth band identified in the regional resolution image does not cross through the high-resolution image, so it remains unverified if the structure at regional resolution is similar to that in the high-resolution images.

### 7.2.4. Medial trough band formation

One suggested formation mechanism for medial trough bands is spreading centered around the axial trough, in a similar fashion to that proposed for the formation of smooth bands (Prockter et al., 2002). A small piece of medial trough band material runs through the high-resolution region (eastern edge), where it appears to consist of 3–4 steep-sided ridges. Nothing about the medial trough band appears smooth at this higher resolution. However, it is important to note that this area appears to have been disrupted and may not accurately represent how a pristine medial trough ridge would appear at high resolution. However, when the high-resolution image is mapped independently, this structure is grouped with the ridge complexes (Section 4.1.2) based on its size, the irregularly spaced ridges and troughs, and the steepness of the ridge flanks. The appearance in the high-resolution images indicates these structures may be an artifact of resolution, only appearing to be smooth because they are a smaller version of a ridge complex.

### 7.2.5. Ridged band formation

Ridged bands are hypothesized to be a version of smooth bands, but with the formation mechanism operating at a different rate

(Tufts et al., 2000; Prockter et al., 2002). Similarly, it is also hypothesized that *ridged bands* form through a tilt-block normal faulting mechanism (Kattenhorn, 2002). This may be the case, however it is important to note implications of the observations from the high-resolution images. Though the *ridged band* material that runs through the high-resolution strip in this region is partially disrupted, it is classified in the high-resolution map as part of the *ridge complex* material (see Section 4.1.2). This implies that the two structures are not as different as previously thought and may indicate a similar, if not evolutionary, formational mechanism between the two units. Likewise, similarly steep and relatively symmetric ridge flanks and chevron-shaped cross section of the individual ridges within the *ridged band* suggest that the *ridged bands*, like *ridge complexes*, require a unique formation mechanism instead of being evolved phases of a *double ridge* (Head et al., 1999).

#### 7.2.6. Lineated band formation

Part of a *lineated band* identified in the regional map is exposed in the high-resolution image as *lineated ridge-and-trough* or a subunit of plains material (Section 4.2.3). At high resolution, a *lineated band* is dissimilar to a *ridged band*, as the topographic relief of the individual ridges is significantly smaller and the morphology of the ridges differs greatly (Section 4.2.3). Additionally, the spacing and size of the ridges between the observed *ridged bands* (~500 m wide) and the *lineated bands* (~100–200 m wide) are too different to reconcile with proposed degradation. As such, the high-resolution observations suggest that the formation mechanism for *lineated band* material is not the degradation of a *ridged band* as previously proposed (Figueredo and Greeley, 2004). However, because this is the only *lineated band* imaged at this resolution at present, we cannot rule this hypothesis out completely.

#### 7.2.7. Single ridges

The one *single ridge* that was identified in the regional resolution that crosses through the high-resolution frames is identified as a *double ridge* in the high-resolution image. We suspect that *single ridges* are artifacts of the lower, regional resolution, as there are no *single ridges* identified in the high-resolution images. In general, *single ridges* are also thought to either evolve to or from *double ridges* (Section 4.1.1, Greeley et al., 2000), though there is no evidence to support this in the limited high-resolution area, given there are no *single ridges* to observe.

#### 7.3. Surface evolution from inferred stratigraphy

Understanding of the evolution of Europa's surface from direct observation is limited by its surface age, or the past ~60 Ma +/- a factor of 3 (Zahnle et al., 2003). By determining how the visible surface has evolved, we constrain how the resurfacing processes have changed with time by investigating crosscutting structures. Fig. 14 contains examples of analyzing crosscutting relationships to determine relative age.

The purpose of mapping the high-resolution images with both geomorphological and structural focus is to investigate surface morphology and the kinematic origin of structures (thus, resurfacing processes). Part of analyzing the formation of the surface is to investigate how it evolved into what it is like today. We do this by determining crosscutting relationships; however, this method is non-ideal in this region given its limited extent and considering the possibility of reactivation of some structures by tidal forcing. Moreover, comparing the relative ages of structures at the opposite ends of the high-resolution strip is difficult (i.e. we cannot ascertain relative ages for features along the strip because they never come into contact with each other). Thus, we create an evolution of the high-resolution surface that depicts a possible sequence of events, but requires further investigation and comparison to other

high-resolution regions. It is important to note that not all features within an inferred "step" necessarily formed contemporaneously, but in the same general timeframe (Fig. 15).

The inferred stratigraphic column (Fig. 16) of this region is, from oldest to youngest: *ridged plains*, *bands* and other *lineaments*, *chaos*, and *fractures*. This sequence matches closely with those inferred in other regions of Europa at the regional scale (Pappalardo et al., 1999; Prockter et al., 1999; Figueredo and Greeley, 2000, 2004; Greeley et al., 2000). These time periods of formation blend into one another, but there are a few exceptions to this stratigraphy, especially in the relative ages of some lineaments (Geissler et al., 1998). In general, however, this progression of surface features holds. In terms of landscape degradation is some evidence of segregation (Spencer, 1987; e.g. Fig. 7, dark material in troughs) but no apparent sublimation features (Moore et al., 1999; 2009). Thus, our results support the possibility that this evolution of features is an indication of possible changes in the thickness of the ice shell (Pappalardo et al., 1999). Whether this is a cyclical process (Husmann and Spohn, 2004) or not remains unclear.

The high-resolution images do confirm how the relative ages inferred from regional resolution images may not be accurate. For example, a few works have used lineaments and bands crossing through chaos region as an indication that these lineaments are younger than the chaos terrain (Greenberg et al., 1999; Figueredo and Greeley, 2000). If we had only analyzed the regional resolution, we may have thought this as well because there exist features that cross through the chaos. However, it becomes evident in the high-resolution images that these structures have weathered the formation of the chaos region around them (Fig. 9; Prockter and Schenk, 2005). Thus, considering the high-resolution data is crucial to the accurate determination of what we are actually observing at the regional resolution. Further high-resolution data is needed to confirm these findings though, as we only directly observe local relationships with this single, narrow strip of high-resolution images.

#### 7.4. Distributed to discrete deformation

As previously alluded to, the structural relationships summarized in Figs. 14–16 evolve from small-scale ridge-and-trough systems to scarp and chaos terrain formation, with features like double and complex ridges occurring mostly in the middle of the stratigraphic column and rarely throughout. Thus, the high-resolution surface is consistent with the hypothesis that Europa resurfacing has changed through time (Pappalardo et al., 1999). We concur, as previously concluded by Figueredo and Greeley (2004), that the style of deformation has changed from distributed to discrete. From this, we infer that Europa's icy lithosphere has strengthened with time, presumably due to cooling and thickening. This hypothesis can account for the observed structural relationships and the surface structure formation hypotheses that we favor based on the high-resolution mapping. *Ridge-and-trough* terrain forming by folding is a distributed deformation mechanism (Section 7.1.1), bands could be formed by a combination of distributed and discrete deformation (e.g., Patterson et al., 2006), *double ridges* formed by compaction or linear diapirism (Section 7.1.2), chaos formed by lens collapse or diapirism (Section 7.1.3) are all forms of discrete deformation. Additionally, ice shell thickening would initially result in compressive forces before extensional forces dominate (Nimmo, 2004) which would explain the transition from compressional folds to extensional bands. Whether this activity is cyclic or occurred recently (within the age of the surface), we cannot say from this analysis.

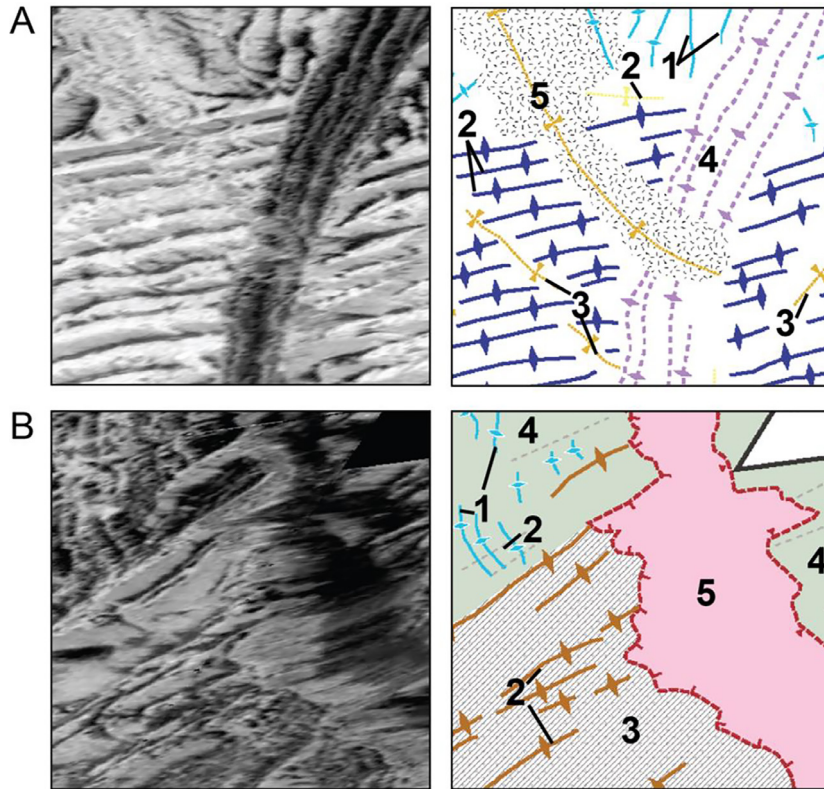


**Fig. 14.** Examples of crosscutting relationships used to determine relative ages, as labeled by the numbers where 1 is the oldest event and 5 is the youngest event. In frame (A) the relationships are as follows: (1) the *subdued ridge-and-trough* terrain is cut by (2) the *ridge-and-trough* terrain which is cut by (3) a few *minor troughs* which are intersected by (4) the *ropy ridge* which is cut by (5) a *minor trough* and *high albedo smooth material*. In (B) the cross-cutting relationships are as follows: (1) the *subdued ridge-and-trough* terrain is cut by (2) *fine lineaments* and *subdued ridge complex* structure covered by (3) a *low albedo smooth material* which is modified by (4) *chaos formation* which is cut by a (5) *scarp structure*. While these two areas do not overlap, we can draw general inferences on the overall history of the region as a whole by observing the trends in the local crosscutting relationships—for example, *subdued ridge-and-trough* terrain is always the oldest and *scarps* are some of the youngest features—which lead to the stratigraphic history displayed in Figs. 15 and 16.

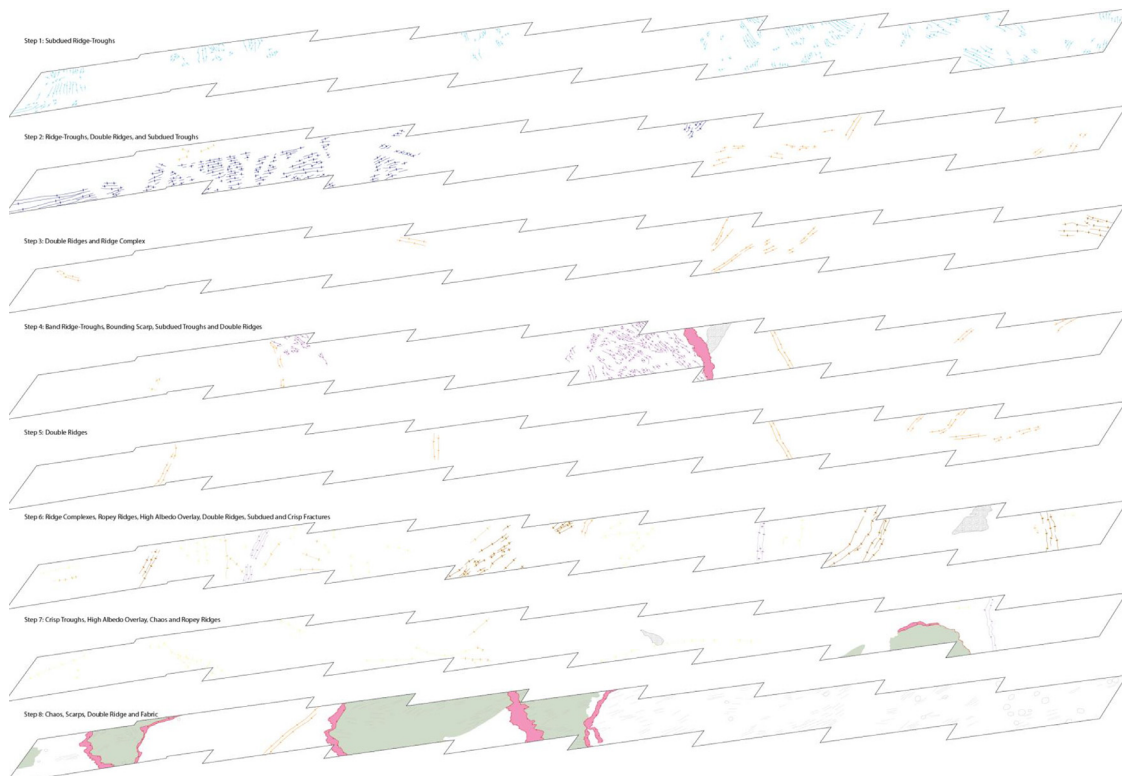


**Fig. 15.** Inferred history of this region determined by crosscutting relationships to determine the relative age of the structures.

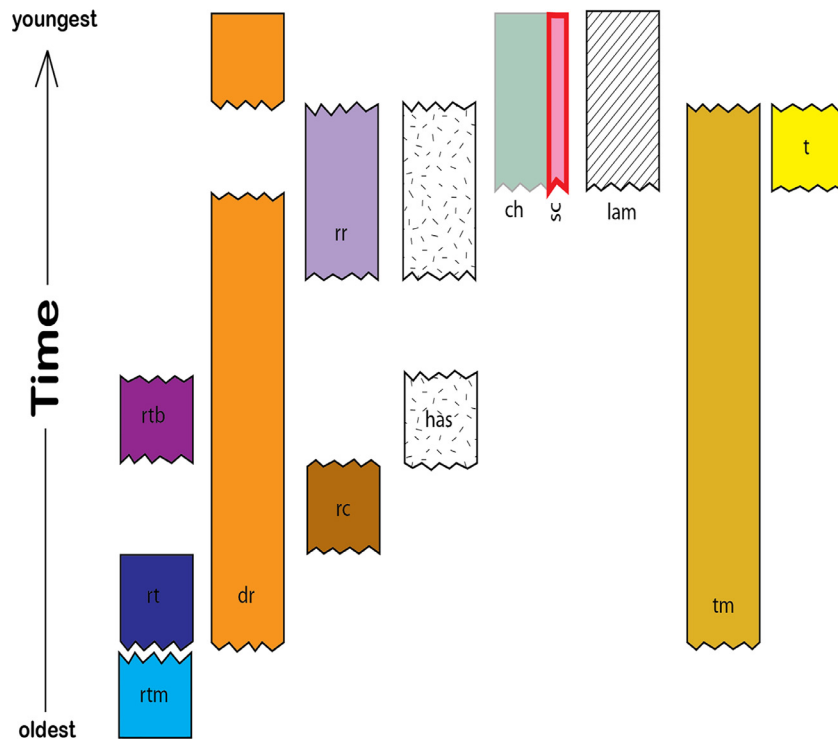


Fig. 16. Stratigraphic column determined by crosscutting relationships among units from the evolutionary sequence (Fig. 14). Unit abbreviations from Structural Map (Fig. 3(C)).

## 8. Conclusions

Through key high-resolution observations obtained by mapping the E12 Mottle region in detail, we constrain the formation mechanism for structures on Europa. Our findings include:

1. Ridge-and-trough systems are observed to be multi-generational, and to have regular spacing and symmetric, gentle slopes, favoring the folds formation hypothesis.
2. *Double ridges* are remarkably consistent in size and shape along their length, favoring the compaction or linear diapirism hypotheses, though neither fits perfectly.
3. Chaos terrain has sharp boundaries, preserved pre-existing structures and heavily deformed border regions, suggesting that the water lens collapse hypothesis is the most likely formation mechanism.
4. Different morphological types of bands could have different formation mechanisms, not necessary related to the evolution of *double ridges* or to the same mechanism operating at different rates. If they are formed by the same mechanism, the significant morphological differences need to be explained (cf, Howell and Pappalardo, in prep).
5. The *high albedo smooth* morphological terrain unit may originate from frosting due to cryovolcanic deposits, thermal processes, or impact ejecta. However, we propose that this is likely a new material not identified previously, which appears smooth at 8–16 m/pixel but likely has structure on a smaller scale only visible at a higher resolution.
6. This region of Europa's surface is covered in small (<50 m diameter) pits, which we interpret, based on their distribution, as secondary craters. The high-resolution region closest (~50 km) to the primary crater appears to have undergone modification (not associated with chaos as identified in the regional map), and the pre-existing structures are heavily degraded compared to the surrounding terrain, possibly indicating that secondary craters could aid in resurfacing small patches of Europa.

7. *Single ridges* are not observed in the high-resolution mosaic despite identification in the overlapping regional resolution image. This could indicate that *single ridges* are an artifact of low resolution and will be reclassified when higher-resolution images become available.
8. At the scale of the high-resolution images, Europa's surface has numerous *fine lineations*, possibly a result of tectonic loading or the presence of a tectonic fabric.

Resurfacing on Europa has transitioned from distributed deformation, seen in the multiple generations of ridge-and-trough systems, to discrete—including ridges, chaos features, scarps, and troughs. We predict that remnants of the distributed deformation, such as a tectonic fabric, will become apparent with higher resolution images from Europa Clipper. Ultimately, the shift in deformation from distributed to discrete may be driven by ice-shell thickening over the visible surface age.

## Acknowledgments

We thank D. Alex Patthoff and Cynthia Phillips for useful discussions throughout the course of this work. We also thank David Senske, Francis Nimmo, Paul Helfenstein, and an anonymous reviewer for helpful comments that improved the quality of this manuscript. Mosaics were made by the first author using data from the NASA PDS and processed using ISIS3. This work was supported by the Furukawa Memorial Fellowship at UCLA and by NASA Headquarters under the NASA Earth and Space Science Fellowship Program – Grant 80NSSC17K0602. Portions of this research were carried out at the Jet Propulsion Laboratory, California Institute of Technology, under contract with the National Aeronautics and Space Administration.

## References

- Aydin, A., 2006. Failure modes of the lineaments on Jupiter's moon, Europa: implications for the evolution of its icy crust. *J. Struct. Geol.* 28, 2222–2236.

- Banerdt, W.B., Golombek, M.P., Tanaka, K.L., 1992. Stress and tectonics on Mars. *Mars* 249–297.
- Bierhaus, E.B., Chapman, C.R., Merline, W.J., 2005. Secondary craters on Europa and implications for cratered surfaces. *Nat. Lett.* 437, 1125–1127.
- Bierhaus, E.B., Chapman, C.R., Merline, W.J., Brooks, S.M., Asphaug, E., 2001. Pwyll secondaries and other small craters on Europa. *Icarus* 153, 264–276.
- Boyce, J.M., Wilson, L., Mouginiis-Mark, P.J., Hamilton, C.W., Tornabene, L.L., 2012. Origin of small pits in martian impact craters. *Icarus* 221, 262–275.
- Carr, M.H., Belton, M.J.S., Chapman, C.R., Davies, M.E., Geissler, P., Greenberg, R., McEwen, A.S., Tufts, B.R., Greeley, R., Sullivan, R., Head, J.W., Pappalardo, R.T., Klaasen, K.P., Johnson, T.V., Kaufman, J., Senske, D., Moore, J., Neukum, G., Schubert, G., Burns, J.A., Thomas, P., Veverka, J., 1998. Evidence for a subsurface ocean on Europa. *Nature* 391, 363–365.
- Collins, G.C., McKinnon, W.B., Moore, J.M., Nimmo, F., Pappalardo, R.T., Prockter, L.M., Schenk, P.M., 2009. Tectonics of the outer planet satellites. *Planet. Tecton.* 11, 264–350.
- Crawford, G.D., Stevenson, D.J., 1988. Gas-driven water volcanism and the resurfacing of Europa. *Icarus* 73, 66–79.
- Culha, C., Hayes, A.G., Manga, M., Thomas, A.M., 2014. Double ridges on Europa accommodate some of the missing surface contraction. *J. Geophys. Res. Planets* 119, 395–403.
- Dalton, J.B., Shirley, J.H., Kamp, L.W., 2012. Europa's icy bright plains and dark lineae: exogenic and endogenic contributions to composition and surface properties. *J. Geophys. Res. Planets* 117.
- Denevi, B.W., Blewett, D.T., Buczkowski, D.L., Capaccioni, F., Capria, M.T., De Sanctis, M.C., Garry, W.B., Gaskell, R.W., Le Corre, L., Li, J.Y., Marchi, S., McCoy, T.J., Nathues, A., O'Brien, D.P., Petro, N.E., Pieters, C.M., Preusker, F., Raymond, C.A., Reddy, V., Russell, C.T., Schenk, P., Scully, J.E., Sunshine, J.M., Tosi, F., Williams, D.A., Wyrick, D., 2012. Pitted terrain on Vesta and Implications for the presence of volatiles. *Science* 338, 246–249.
- Doggett, T., Greeley, R., Figueredo, P., 2009. Geologic stratigraphy and evolution of Europa's surface. In: Pappalardo, R.T., McKinnon, W.B., Khurana, K.K. (Eds.), *Europa*. The University of Arizona Press, Tucson, pp. 137–159.
- Dombard, A.J., Patterson, G.W., Lederer, A.P., Prockter, L.M., 2013. Flanking fractures and the formation of double ridges on Europa. *Icarus* 223, 74–81.
- Fagents, S.A., 2003. Considerations for effusive cryovolcanism on Europa: the post-Galileo perspective. *J. Geophys. Res. Planets* 108.
- Fagents, S.A., Greeley, R., 1997. Explosive venting on Europa? A preliminary assessment. In: *Proceedings of the Lunar and Planetary Science Conference XXVIII Abstract 1196*.
- Ferrill, D.A., Wyrick, D.Y., Smart, K.J., 2011. Coseismic, dilational-fault and extension-fracture related pit chain formation in Iceland: Analog for pit chains on Mars. *Lithosphere* 3, 133–142.
- Figueredo, P.H., Greeley, R., 2004. Resurfacing history of Europa from pole-to-pole geological mapping. *Icarus* 167, 287–312.
- Figueredo, P.H., Greeley, R., 2000. Geologic mapping of the northern leading hemisphere of Europa from Galileo solid-state imaging data. *J. Geophys. Res. Planets* 105, 22629–22646.
- Geissler, P.E., Greenberg, R., Hoppa, G., McEwen, A., Tufts, R., Phillips, C., Clark, B., Ockert-Bell, M., Helfenstein, P., Burns, J., Veverka, J., Sullivan, R., Greeley, R., Pappalardo, R.T., Head, J.W., Belton, M.J.S., Denk, T., 1998. Evolution of lineaments on Europa: clues from Galileo multispectral imaging observations. *Icarus* 135, 107–126.
- Gillis-Davis, J.J., Blewett, D.T., Gaskell, R.W., Denevi, B.W., Robinson, M.S., Strom, R.G., Solomon, S.C., Sprague, A.L., 2009. Pit-floor craters on Mercury: evidence of near-surface igneous activity. *Earth Planet. Sci. Lett.* 285, 243–250.
- Greeley, R., Figueredo, P.H., Williams, D.A., Chuang, F.C., Klemaszewski, J.E., Kadel, S.D., Prockter, L.M., Pappalardo, R.T., Head, J.W., Collins, G.C., Spaul, N.A., Sullivan, R.J., Moore, J.M., Senske, D.A., Tufts, B.R., Johnson, T.V., Belton, M.J.S., Tanaka, K.L., 2000. Geologic mapping of Europa. *J. Geophys. Res. Planets* 105, 22559–22578.
- Greenberg, R., Geissler, P., 2002. Europa's dynamic icy crust. *Meteorit. Planet. Sci.* 37, 1685–1710.
- Greenberg, R., Geissler, P., Hoppa, G., Tufts, B.R., Durda, D.D., Pappalardo, R.T., Head, J.W., Greeley, R., Sullivan, R., Carr, M.H., 1998. Tectonic processes on Europa: tidal stresses, mechanical response, and visible features. *Icarus* 135, 64–78.
- Greenberg, R., Hoppa, G.V., Tufts, B.R., Geissler, P., Riley, J., Kadel, S.D., 1999. Chaos on Europa. *Icarus* 141, 263–286.
- Greenberg, R., Sak, P.B., 2014. The ridges of Europa: Extensions of adjacent topography onto their flanks. *Earth Planet. Sci. Lett.* 389, 43–51.
- Han, L., Melosh, H.J., 2010. Origin of Europa's ridges by incremental ice-wedging. *Am. Geophys. Union Fall Meet.* 2010, Abstr. #P33B-1577.
- Han, L., Showman, A.P., 2008. Implications of shear heating and fracture zones for ridge formation on Europa. *Geophys. Res. Lett.* 35.
- Head, J.W., Pappalardo, R.T., Sullivan, R., 1999. Europa: morphological characteristics of ridges and triple bands from Galileo data (E4 and E6) and assessment of a linear diapirism model. *J. Geophys. Res. Planets* 104, 24223–24236.
- Head, J.W., Sherman, N.D., Pappalardo, R.T., Greeley, R., Sullivan, R., Senske, D., McEwen, A., 1998. Geologic history of the E4 region of Europa: implications for ridge formation, cryovolcanism, and chaos formation. In: *Proceedings of the Lunar and Planetary Science Conference XXIX Abstract 1412*.
- Helfenstein, P., Parmentier, E.M., 1983. Patterns of fracture and tidal stresses on Europa. *Icarus* 53, 415–430.
- Helfenstein, P., Currier, N., Clark, B.E., Veverka, J., Bell, M., Sullivan, R., Klemaszewski, J., Greeley, R., Pappalardo, R.T., Head III, J.W., Jones, T., 1998. Galileo observations of Europa's opposition effect. *Icarus* 135, 41–63.
- Hurford, T.A., Beyer, R.A., Schmidt, B., Preblich, B., Sarid, A.R., Greenberg, R., 2005. Flexure of Europa's lithosphere due to ridge-loading. *Icarus* 177, 380–396.
- Husmann, H., Spohn, T., 2004. Thermal-orbital evolution of Io and Europa. *Icarus* 171, 391–410.
- Johnston, S.A., Montési, L.G.J., 2014. Formation of ridges on Europa above crystallizing water bodies inside the ice shell. *Icarus* 237, 190–201.
- Johnston, S.A., Montési, L.G.J., 2017. The impact of a pressurized regional sea or global ocean on stresses on Enceladus. *J. Geophys. Res. Planets* 122, 1258–1275.
- Kadel, S.D., Fagents, S.A., Greeley, R., 1998. Trough-bounding ridge pairs on Europa—considerations for an endogenic model of formation. In: *Proceedings of the Lunar and Planetary Science Conference XXIX Abstract 1078*.
- Kattenhorn, S.A., 2002. Nonsynchronous rotation evidence and fracture history in the bright plains region, Europa. *Icarus* 157, 490–506.
- Kattenhorn, S.A., Prockter, L.M., 2014. Evidence for subduction in the ice shell of Europa. *Nat. Geosci.* 7, 762–767.
- Kattenhorn, S., Hurford, T., 2009. Tectonics of Europa. In: Pappalardo, R.T., McKinnon, W.B., Khurana, K.K. (Eds.), *Europa*. The University of Arizona Press, Tucson, pp. 199–236.
- Leonard, E.J., Yin, A., Pappalardo, R.T., 2015. Structural analysis of very high-resolution Galileo images of Europa: implications for surface evolution. In: *Proceedings of the Lunar and Planetary Science Conference XLVI Abstract 2429*.
- Lucchitta, B.K., Soderblom, L.A., 1982. The geology of Europa. In: *Satellites of Jupiter*. University of Arizona Press, Tucson, AZ, pp. 521–555.
- Malin, M.C., Pieri, D.C., 1986. *Europa, Satellites* JA Burns, MS Matthews. University of Ariz. Press, Tucson, pp. 689–717.
- Martin, E.S., Kattenhorn, S.A., Collins, G.C., Michaud, R.L., Pappalardo, R.T., Wyrick, D.Y., 2017. Pit chains on Enceladus signal the recent tectonic dissection of the ancient cratered terrains. *Icarus* 294, 209–217.
- McEwen, A.S., Bierhaus, E.B., 2006. The importance of secondary cratering to age constraints on planetary surfaces. *Earth Planet. Sci.* 34, 535–567.
- Melosh, H.J., Turtle, E.P., 2004. Ridges on Europa: origin by incremental ice-wedging. In: *Proceedings of the Lunar and Planetary Science Conference XXXV Abstract 2029*.
- Michaut, C., Manga, M., 2014. Domes, pits, and small chaos on Europa produced by water sills. *J. Geophys. Res. Planets* 119, 550–573.
- Moore, J.M., Asphaug, E., Morrison, D., Spencer, J.R., Chapman, C.R., Bierhaus, B., Sullivan, R.J., Chuang, F.C., Klemaszewski, J.E., Greeley, R., Bender, K.C., 1999. Mass movement and landform degradation on the icy Galilean satellites: Results of the Galileo nominal mission. *Icarus* 140, 294–312.
- Moore, J.M., Black, G., Buratti, B., Phillips, C.B., Spencer, J., Sullivan, R., 2009. Surface Properties, Regolith, and Landscape Degradation. University of Arizona Press, Tucson, pp. 329–349.
- Moore, J.M., Howard, A.D., Umurhan, O.M., White, O.L., Schenk, P.M., Beyer, R.A., McKinnon, W.B., Spencer, J.R., Grundy, W.M., Lauer, T.R., Nimmo, F., 2017. Sublimation as a landform-shaping process on Pluto. *Icarus* 287, 320–333.
- Nimmo, F., Gaidos, E., 2002. Strike-slip motion and double ridge formation on Europa. *J. Geophys. Res. Planets* 107, 5.
- Nimmo, F., Giese, B., Pappalardo, R.T., 2003. Estimates of Europa's ice shell thickness from elastically-supported topography. *Geophys. Res. Lett.* 30.
- Nimmo, F., 2004. Stresses generated in cooling viscoelastic ice shells: application to Europa. *Geophys. Res. Planets* 109, 30.
- O'Brien, D., Geissler, P.E., Greenberg, R., 2002. A Melt-through Model for Chaos Formation on Europa. *Icarus* 156, 152–161.
- Okubo, C.H., Martel, S.J., 1998. Pit crater formation on Kilauea volcano, Hawaii. *J. Volcanol. Geotherm. Res.* 86.
- Pappalardo, R.T., Barr, A.C., 2004. The origin of domes on Europa: the role of thermally induced compositional diapirism. *Geophys. Res. Lett.* 31.
- Pappalardo, R.T., Belton, M.J.S., Breneman, H.H., Carr, M.H., Chapman, C.R., Collins, G.C., Denk, T., Fagents, S., Geissler, P.E., Giese, B., Greeley, R., Greenberg, R., Head, J.W., Helfenstein, P., Hoppa, G., Kadel, S.D., Klaasen, K.P., Klemaszewski, J.E., Magee, K., McEwen, A.S., Moore, J.M., Moore, W.B., Neukum, G., Phillips, C.B., Prockter, L.M., Schubert, G., Senske, D.A., Sullivan, R.J., Tufts, B.R., Turtle, E.P., Wagner, R., Williams, K.K., 1999. Does Europa have a subsurface ocean? Evaluation of the geological evidence. *J. Geophys. Res. Planets* 104, 24015–24055.
- Pappalardo, R.T., Greeley, R., 1995. A review of the origins of subparallel ridges and troughs: Generalized morphological predictions from terrestrial models. *J. Geophys. Res. Planets* 100, 18985–19007.
- Pappalardo, R.T., Head, J.W., Greeley, R., Sullivan, R.J., Piicher, C., Schubert, G., Moore, W.B., Carr, M.H., Moore, J.M., Belton, M.J.S., Goldsby, D.L., 1998a. Geological evidence for solid-state convection in Europa's ice shell. *Let. Nat.* 391, 365–368.
- Pappalardo, R.T., Head, J.W., Sherman, N.D., Greeley, R., Sullivan, R.J., 1998b. Classification of European ridges and troughs and a possible genetic sequence. In: *Proceedings of the Lunar and Planetary Science Conference XXIX Abstract 1859*.
- Patel, J.G., Pappalardo, R.T., Prockter, L.M., Collins, G.C., Head, J.W., 1999a. Morphology of ridge and trough terrain on Europa: fourier analysis and comparison to ganymede. *Eos Trans. AGU* 80 (17), Spring Meet. Suppl., S210.
- Patel, J.G., Pappalardo, R.T., Head, J.W., Collins, G.C., Hiesinger, H., Sun, J., 1999b. Topographic wavelengths of Ganymede groove lanes from Fourier analysis of Galileo images. *J. Geophys. Res.* 104, 24057–24074.
- Patterson, G.W., Head, J.W., Pappalardo, R.T., 2006. Plate motion on Europa and non-rigid behavior of the icy lithosphere: the Castalia Macula region. *J. Struct. Geol.* 28, 2237–2258.

- Phillips, C.B., McEwen, A.S., Hoppa, G.V., Fagents, S.A., Greeley, R., Klemaszewski, J.E., Pappalardo, R.T., Klaasen, K.P., Breneman, H.H., 2000. The search for current geologic activity on Europa. *J. Geophys. Res. Planets* 105 (E9), 22579–22597.
- Prockter, L., Schenk, P., 2005. Origin and evolution of Castalia Macula, an anomalous young depression on Europa. *Icarus* 177, 305–326.
- Prockter, L.M., 2004. Europa at the highest resolution: implications for surface processes and landing sites. In: *Proceedings of the Lunar and Planetary Science Conference XXXV*. Abstract 1409.
- Prockter, L.M., Antman, A.M., Pappalardo, R.T., Head, J.W., Collins, G.C., 1999. Europa: Stratigraphy and geological history of the anti-Jovian region from Galileo E14 solid-state imaging data. *J. Geophys. Res. Planets* 104, 16531–16540.
- Prockter, L.M., Figueredo, P.H., Pappalardo, R.T., Head, J.W., Collins, G.C., 2000. Geology and mapping of dark terrain on Ganymede and implications for grooved terrain formation. *J. Geophys. Res. Planets* 105, 22519–22540.
- Prockter, L.M., Head, J.W., Pappalardo, R.T., Sullivan, R.J., Clifton, A.E., Giese, B., Wagner, R., Neukum, G., 2002. Morphology of European bands at high resolution: a mid-ocean ridge-type rift mechanism. *J. Geophys. Res. Planets* 107.
- Prockter, L.M., Pappalardo, R.T., 2000. Folds on Europa: implications for crustal cycling and accommodation of extension. *Science* 289, 941–943.
- Schenk, P.M., 2009. Slope characteristics of Europa: constraints for landers and radar Sounding. *Geophys. Res. Lett.* 36.
- Schenk, P.M., 2002. Thickness constraints on the icy shells of the galilean satellites from a comparison of crater shapes. *Lett. Nat.* 417, 419–421.
- Schenk, P.M., McKinnon, W.B., 1989. Fault offsets and lateral crustal movement on Europa: Evidence for a mobile ice shell. *Icarus* 79.
- Schenk, P.M., Pappalardo, R.T., 2004. Topographic variations in chaos on Europa: implications for diapiric formation. *Geophys. Res. Lett.* 31.
- Schenk, P.M., Turtle, E.P., 2009. Europa's impact craters: probes of the icy shell. In: Pappalardo, R.T., McKinnon, W.B., Khurana, K.K. (Eds.), *Europa*. The University of Arizona Press, Tucson, pp. 181–198.
- Schmidt, B.E., Blankenship, D.D., Patterson, G.W., Schenk, P.M., 2011. Active formation of 'chaos terrain' over shallow subsurface water on Europa. *Nature* 479, 502–505.
- Schmidt, K.G.K., Dahl-Jensen, D., 2003. An ice crystal model for Jupiter's moon Europa. *Ann. Glaciol.* 37, 129–133.
- Shirley, J.H., Dalton, J.B., Prockter, L.M., Kamp, L.W., 2010. Europa's ridged plains and smooth low albedo plains: Distinctive compositions and compositional gradients at the leading side-trailing side boundary. *Icarus* 210, 358–384.
- Soderlund, K.M., Schmidt, B.E., Wicht, J., Blankenship, D.D., 2013. Ocean-driven heating of Europa's icy shell at low latitudes. *Nat. Geosci. Lett.* 7, 16–19.
- Spaun, N.A., Pappalardo, R.T., Head, J.W., 2003. Evidence for shear failure in forming near-equatorial lineae on Europa. *J. Geophys. Res. Planets* 108.
- Spencer, J.R., 1987. Thermal segregation of water ice on the Galilean satellites. *Icarus* 69 (2), 297–313.
- Sullivan, R., Greeley, R., Homan, K., Klemaszewski, J., Belton, M.J.S., Carr, M.H., Chapman, C.R., Tufts, R., Head, J.W., Pappalardo, R., Moore, J., Thomas, P., Team, G.I., 1998. Episodic plate separation and fracture infill on the surface of Europa. *Lett. Nat.* 391, 371–373.
- Sullivan, R., Moore, J., Pappalardo, R., 1999. Mass-wasting and slope evolution on Europa. In: *Proceedings of the Lunar and Planetary Science Conference XXX*. Abstract 1747.
- Thomas, P., Veverka, J., Bloom, A., Duxbury, T., 1979. Grooves on Phobos: their distribution, morphology and possible origin. *J. Geophys. Res. Solid Earth* 84, 8457–8477.
- Tornabene, L.L., Osinski, G.R., McEwen, A.S., Boyce, J.M., Bray, V.J., Caudill, C.M., Grant, J.A., Hamilton, C.W., Mattson, S., Mouginis-Mark, P.J., 2012. Widespread crater-related pitted materials on Mars: further evidence for the role of target volatiles during the impact process. *Icarus* 220, 348–368.
- Tufts, B.R., Greenberg, R., Hoppa, G., Geissler, P., 2000. Lithospheric dilation on Europa. *Icarus* 146, 75–97.
- Vasavada, A., 1999. Near-Surface temperatures on mercury and the Moon and the stability of polar ice deposits. *Icarus* 141, 179–193.
- Vincent, J.B., Bodewits, D., Besse, S., Sierks, H., Barbieri, C., Lamy, P., Rodrigo, R., Koschny, D., Rickman, H., Keller, H.U., Agarwal, J., 2015. Large heterogeneities in comet 67P as revealed by active pits from sinkhole collapse. *Nature* 523, 63.
- Watters, T.R., Robinson, M.S., Banks, M.E., Tran, T., Denevi, B.W., 2012. Recent extensional tectonics on the Moon revealed by the lunar reconnaissance orbiter camera. *Nat. Geosci.* 5, 181–185.
- Wyrick, D., Ferrill, D.A., Morris, A.P., Colton, S.L., Sims, D.W., 2004. Distribution, morphology, and origins of Martian pit crater chains. *J. Geophys. Res.* 109.
- Zahnle, K., Dones, L., Levison, H.F., 1998. Cratering rates on the Galilean satellites. *Icarus* 136, 202–222.
- Zahnle, K., Schenk, P., Levison, H., Dones, L., 2003. Cratering rates in the outer solar system. *Icarus* 163, 263–289.